National Roadmap for Adaptation 2100
Portuguese Territorial Climate Change Vulnerability Assessment for XXI Century

REPORT

WP4 – Sectoral Impacts Modelling

Forest Fires

Final Version

National Roadmap for Adaptation 2100

Portuguese Territorial Climate Change Vulnerability Assessment for XXI Century

Title: RNA2100 – Sectoral Impacts Modelling – Forest Fires

Authors: Pedro Matos Soares (coord.), Virgílio Bento, Carlos da Camara, Ana Russo, Daniela Lima, Sílvia Nunes, Rita Cardoso, Miguel Lima, Luana Santos, Ricardo Trigo.

February 2024

This report is a product of the National Roadmap for Adaptation 2100 project.

Through the Agreement on the European Economic Area (EEA), Iceland, Liechtenstein and Norway are partners in the internal market with the Member States of the European Union.

In order to promote a continuous and balanced strengthening of economic and trade relations, the parties to the EEA Agreement have established a and trade relations, the parties to the EEA Agreement established a multi-annual Financial Mechanism, known as the EEA. known as EEA Grants.

The EEA Grants aim to reduce social and economic disparities in Europe and to strengthen bilateral relations between these three countries and the beneficiary countries.

For the 2014-2021 period, a total contribution of 2.8 billion euros has been agreed for 15 beneficiary countries. for 15 beneficiary countries. Portugal will receive 102.7 million euros.

Funded by:

Promoter:

Partners:

Table of Contents

List of Figures

List of Tables

List of Acronyms

BUI	Buildup Index
CDF	Cumulative Distribution Function
CDSR	Cumulative DSR
CFFWIS	Canadian Forest Fire Weather Index System
CHI	Continuous Haines Index
CMIP5	Coupled Model Intercomparison Project – Phase 5
DC	Drought Code
DMC	Duff Moisture Code
DSR	Daily Severity Rating
ECMWF	European Centre for Medium-Range Weather Forecasts
EFFIS	European Forest Fire Information System
EUMETSAT	European Organisation for the Exploitation of Meteorological Satellites
EURO-CORDEX	European branch of the Coordinated Regional Climate Downscaling Experiment
FFMC	Fine Fuel Moisture Code
FRP	Fire Radiative Power
FWI	Fire Weather Index
FWIe	Enhanced Fire Weather Index
GHG	Green House Gas
IP	Iberian Peninsula
IP	Iberian Peninsula
ISI	Initial Spread Index
KDE	Kernel Density Estimation
LSA SAF	EUMETSAT Satellite Application Facility for Land Surface Analysis
MODIS	Moderate Resolution Imaging Spectroradiometer
NBA	Normalized Burned Area
NUTS	Nomenclature of Territorial Units for Statistics
PDF	Probability Distribution Function
RCM	Regional Climate Model
RCP	Representative Concentration Pathway

Executive Summary

This report delves into a comprehensive examination of the likely future meteorological fire danger in Portugal, with a primary focus on the potential impacts of climate change. As part of the overarching National Roadmap for Adaptation XXI, the study employs a sophisticated approach, leveraging a multi-model ensemble comprising 13 Regional Climate Models (RCMs). The assessment centres on two key indices, the widely used Fire Weather Index (FWI) and an enhanced version denoted as FWIe, with the implementation of information about atmospheric instability using the Haines index. This investigation serves as a critical component in the development of adaptation strategies for Portugal, contributing valuable insights to the ongoing discourse on climate change mitigation and resilience.

Key Findings and Insights:

- Geospatial Danger: Through meticulous analysis, the study pinpoints the north-eastern region of Portugal, as exhibiting the most significant increases in meteorological fire danger. This geographical specificity enables a nuanced understanding of the localised impact of climate change on fire danger.
- Scenario-dependent Dynamics: A noteworthy aspect of the research lies in its revelation of substantial disparities in meteorological fire danger projections among various emission scenarios. The study systematically contrasts the outcomes under different Representative Concentration Pathways (RCPs), emphasising the nuanced implications of strong mitigation efforts (RCP2.6) versus scenarios with limited or no mitigation (RCP4.5 and RCP8.5). This scenario-specific analysis underscores the importance of tailoring adaptation strategies to the projected climate trajectories.
- Temporal Shifts in Danger Periods: Beyond spatial considerations, the research illuminates temporal shifts in the meteorological danger periods. Projections suggest a noteworthy increase in extreme fire danger days during the summer season. Particularly noteworthy is the extension of the danger period into June and, to a lesser extent, September. This temporal dimension adds a layer of complexity to adaptation planning, urging a more nuanced and dynamic approach to danger assessment.
- Probability of Having Megafires: This study points to a larger probability of having megafires in the future, with fires with intensities larger than 1000 MW doubling or even occurring 3 to 3.5 more times than those of the historical period.
- Return Periods of Large Burned Areas: The study further investigates the projected return periods of large burned areas in Portugal and NUTS II regions, considering various emission scenarios and

future periods. Results, focusing on thresholds of 100,000 ha, 150,000 ha, and 200,000 ha, show a significant decrease in return periods for larger burnt areas, especially for RCP 8.5. For Portugal, return periods of 200,000 ha burnt areas decreased from 6-7 years to 1-2 years for RCP 8.5, a threshold particularly relevant as only three years since 1995 surpassed this value. NUTS II Norte and Centro exhibit similar patterns, with a steep increase in the probability of occurrence for large burnt areas. Return periods decrease, indicating a higher frequency of occurrences in RCP 2.6 and RCP 4.5.

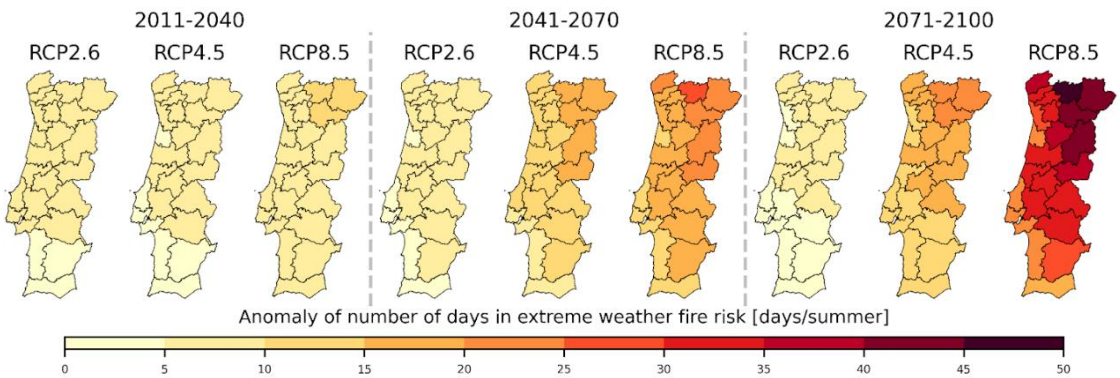

Extended summer average anomaly of number of days with extreme weather fire risk over mainland Portugal for the future periods considering different GHG emission scenarios.

Practical Implications and Recommendations:

- Strategic Adaptation Planning: The study's findings hold profound implications for the formulation of strategic adaptation plans. The identification of regions with heightened danger serves as a crucial guide for directing resources and efforts toward areas where the impact of increased fire danger is anticipated to be most pronounced.
- Scenario-specific Adaptation: The scenario-specific nature of the findings underscores the importance of tailoring adaptation measures to the prevailing emission scenarios. While the heavily mitigated RCP2.6 exhibits relatively modest increases in fire danger, scenarios with less mitigation (RCP4.5 and RCP8.5) demand more robust and targeted adaptation efforts.
- Sensitivity Analysis for Precision: A recommended next step in the research agenda involves a sensitivity analysis, specifically focusing on forest management and understanding the danger of these ecosystems to wildfires. This granular approach aims to enhance the precision of adaptation strategies by accounting for ecosystem-specific dynamics.

- Vegetation Interaction Studies: Acknowledging the pivotal role of vegetation in influencing fire dynamics, future research endeavours should delve into the interaction between meteorological indices (e.g., FWI and FWIe) and vegetation patterns. The incorporation of insights from the latest CMIP6 projections, which include dynamic vegetation components, promises to enrich our understanding of this complex interplay.
- Baseline for Storylines: Integrated into the broader RNA2100 project, this study not only contributes to the scientific discourse but also serves as a practical baseline for the timely preparation of adaptation measures. Its utility extends beyond academia, providing valuable storylines that can be articulated and integrated into the decision-making processes of stakeholders and policymakers.

In conclusion, this research contributes significantly to understanding the intricate dynamics of meteorological fire danger in Portugal. Its multifaceted approach equips stakeholders with actionable insights for effective climate change adaptation and resilience planning, considering both spatial and temporal dimensions, as well as the projected return periods of large burned areas.

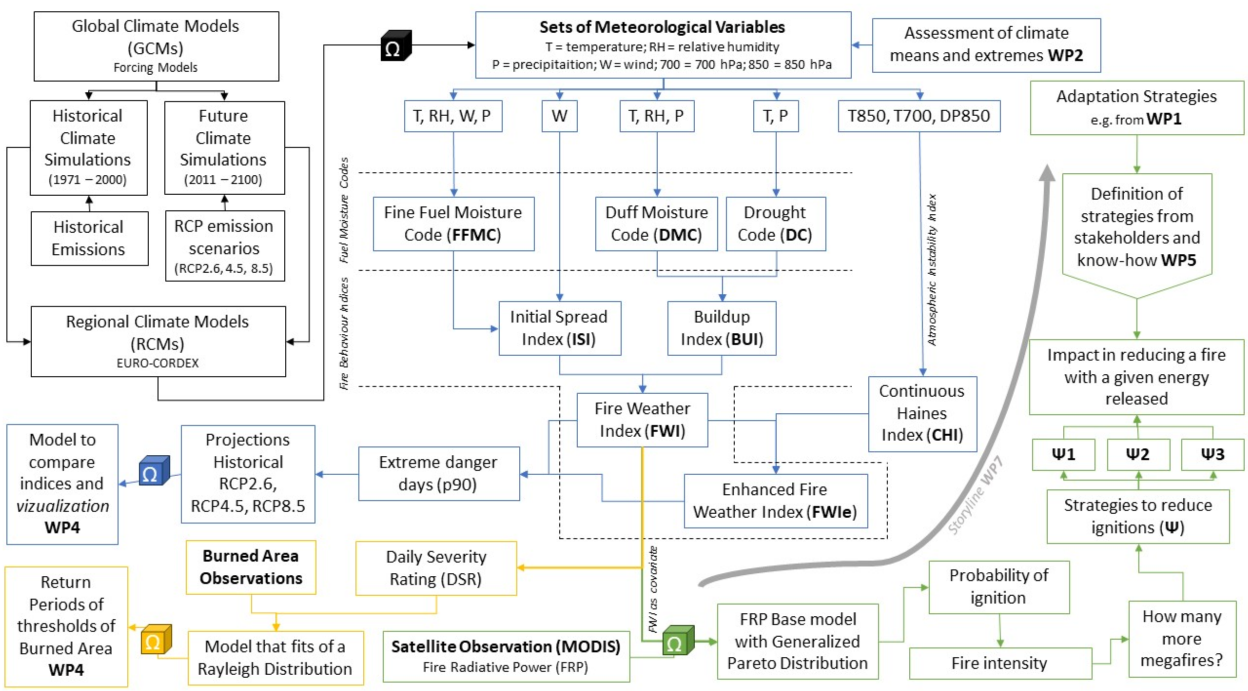

Workflow diagram outlining the activities undertaken within the scope of WP4, illustrating its interconnections with WP5 and WP7.

1. Introduction

Wildfires are some of the most important disturbances to forests and its ecosystems all over the globe, with striking examples in Australia (Boer et al 2020), California (Keeley and Syphard 2021), or the Amazon Forest (Libonati et al 2021). In Europe, the Mediterranean basin represents the most frequently fire-plagued region (Pausas and Fernández-Muñoz 2012), with countries like Portugal (Trigo et al 2006, Turco et al 2019), Spain (Rodrigues et al 2019), Italy (Salis et al 2013), and Greece (Gouveia et al 2016) being recurrently struck by these events. The destructive impacts of wildfires also affect infrastructures, undermining the economy, and threatening human lives and health (Molina-Terrén et al 2019, Oliveira et al 2020, Augusto et al 2020).

One of the most tragic fire seasons of the last decades in south-western Europe was the extended summer season of 2017 in Portugal, where two large fire events, that took place in June and October, were responsible for about 500 thousand hectares of burnt area and more than 110 human fatalities (ICNF 2017). Hence, the characterization and understanding of wildfires and its components has been a major scientific endeavour in the last decades. The highly favourable climate conditions observed in the Iberian Peninsula (IP) are linked to the three main types of wildfires which often occur in the region, namely wind-driven, topographic, and plume-dominated or convective fires. Wind-driven wildfires strongly depend on wind intensity and direction, with small changes in landscape and topography having virtually no impact on fire propagation. Topographic fires are highly dependent on local scale winds caused by differential solar heating (i.e., slope or valley winds and sea breezes) showing a strong day-night intensity change. Plume-dominated (convective) fires are characterized by the presence of intense atmospheric instability allied with the accumulation and availability of fuels for fire development, being normally more intense (energetic) and with unpredictable behaviour.

One of the most well-known and widely used meteorological fire danger indices is the Canadian forest fire weather index system (CFFWIS), which consists of six components that account for the effects of fuel moisture and weather conditions on fire behaviour (Van Wagner 1974). Three of the CFFWIS components rely on empirical relations between meteorological variables (temperature, precipitation, relative humidity, and wind speed) and the stress of a standard fuel that can be described as a generalized Canadian jack pine forest (Stocks et al 1989), which are the fine fuel moisture code (FFMC), Duff moisture code (DMC), and drought code (DC). The remaining three components are the initial spread index (ISI), which is a combination between FFMC and wind speed, the build-up index (BUI), which is a combination between DMC and DC, and finally the fire weather index (FWI), which is a combination between ISI and BUI (Van Wagner 1987). The FWI offers information on how favourable the meteorological conditions are to build up and spread a wildfire, in case an ignition is triggered, and, when calibrated, FWI is particularly suitable to assess meteorological fire danger over Mediterranean Europe (DaCamara et al 2014). Indeed, FWI is now operationally working within the scope of the emergency management services in the EU Copernicus programme – the Fire Danger Forecast module of the European Forest Fire Information System (EFFIS) (San-Miguel-Ayanz et al 2012) –, and within the EUMETSAT Satellite Application Facility for Land Surface Analysis (LSA SAF) (Trigo et al 2011) as part of the Fire Risk Map product. However, despite its versatility and widespread use, it has been stressed that the FWI does not incorporate any component that considers the local (or regional) atmospheric instability, a feature that could be relevant in some regions (Hoinka and De Castro 2003).

A recent work proposed a way forward to alleviate that shortcoming, improving the FWI by the incorporation of atmospheric instability (Pinto et al 2020), through the inclusion of the Continuous Haines Index (CHI). This new enhanced index can be used to ameliorate estimates of the probability of exceedance of energy released by fires. To achieve this, a Generalized Pareto (GP) model was considered, and the authors showed that by using a steplike methodology that allows combining FWI and CHI as covariates of the GP parameters, an improved model is obtained that allows defining an enhanced FWI (hereafter denoted FWIe). For instance, Pinto et al (2020) showed that FWIe may be a relevant source of information in cases of mild FWI associated with very high instability in the atmosphere (high CHI) where the danger is often underestimated, and in cases with very high FWI that can actually be associated to more moderate fire risk due to the presence of a very stable atmosphere (low CHI).

Climate change is expected to affect the frequency and intensity of wildfires in the future (Ruffault et al 2020), which heightens the vulnerability of regions located in Mediterranean climate types. An example is California, where climate change is increasing the likelihood of autumn days with extreme fire weather twofold (Goss et al 2020). Another particularly vulnerable region is Iberia (Sousa et al 2015), a prominent climate change hot spot (Diffenbaugh and Giorgi 2012, Alessandri et al 2014).

With the aim of studying climate change impacts and consequences, at the local and regional scales, experiments to dynamically or statistically downscale global climate models (GCMs) were designed within projects such as the Coordinated Regional Downscaling Experiment (CORDEX) (Giorgi et al 2009, Jacob et al 2020). CORDEX effort aims to deliver frameworks for a coordinated model evaluation and climate projections, and an interface to the users of climate simulations concerning climate change impact, adaptation, and mitigation studies. EURO-CORDEX is the European branch of the CORDEX initiative which produced ensemble climate simulations based on multiple dynamical downscaling models forced by multiple GCMs from the Coupled Model Intercomparison Project Phase 5 (CMIP5). EURO-CORDEX simulations have been widely evaluated for present climate, revealing significant improvements in simulating the temporal and spatial variability of the European climate (Vautard et al 2013, Kotlarski et al

2014, Katragkou et al 2015, Prein et al 2016). Recently, Herrera et al (2020) assessed the skill of EURO-CORDEX Regional Climate Models (RCMs) in representing the precipitation and temperature over the Iberian Peninsula, showing a good spatial agreement among simulations and observations. A similar assessment was performed by Soares et al. (2017a) and Cardoso et al. (2019) over Portugal, revealing a good agreement between the multi-model EURO-CORDEX ensemble and observations, with substantial gains when compared to previous regional climate projects like PRUDENCE and ENSEMBLES (Soares et al 2012).

The added value of using high-resolution EURO-CORDEX simulations was quantified for the first time by Soares and Cardoso (2018), revealing significant added value in the representation of precipitation patterns over Europe, particularly for extremes. More recently, the same method was applied for temperature and wind over Europe (Cardoso and Soares 2022), and for precipitation and temperature over the Iberian Peninsula (Careto et al 2022a, 2022b). EURO-CORDEX RCMs were also able to represent the near-surface wind speed onshore (Moemken et al 2018, Nogueira et al 2019, Vautard et al 2013) and offshore (Soares et al 2017b). Based on a large ensemble of continental-scale simulations from EURO-CORDEX, several works focused on the assessment of changes induced by global warming on key wildfire-related meteorological variables, such as precipitation (Jacob et al 2014, Prein et al 2016, Soares et al 2017a), temperature (Vautard et al 2013, Jacob et al 2014, Cardoso et al 2019), and wind (Soares et al 2017b, Nogueira et al 2019) in the Iberian Peninsula. These studies have steadily projected a decrease in mean precipitation, together with an increase in extreme precipitation events (Soares et al 2017a); a significant increase in maximum and minimum temperatures spanning all seasons and emission scenarios (Cardoso et al 2019); and a reduction in 10-m wind speed over northern Portugal during winter and autumn (Nogueira et al 2019), whilst a small increase during summer over central Portugal. Furthermore, several works have taken advantage of the CORDEX multi-model approach to directly analyze future projections of wildfire risk in different regions (Faggian 2018, Varela et al 2019, Fargeon et al 2020, Ruffault et al 2018, Trnka et al 2021). A recent work (Calheiros et al 2021) focusing on the Iberian Peninsula, used EURO-CORDEX models to assess the impact of climate change on the spatial distribution of clusters by taking advantage of CFFWIS components. However, Calheiros et al (2021) only looked at RCP4.5 and RCP8.5[1], lacking the heavily mitigated RCP2.6, which is also relevant in terms of adaptation measures.

The Iberian Peninsula fire regime is particularly susceptible to weather and climate variability, where extreme events such as heatwaves and droughts, and anomalous atmospheric circulation patterns are typically associated with high incidence of fires (Pereira et al 2005, Russo et al 2017, Parente et al 2019).

[1] Representative Concentration Pathways (RCPs) are scenarios used in climate modeling and research to project future greenhouse gas concentrations and their potential impacts on the climate system. RCPs represent different greenhouse gas concentration trajectories that are used as inputs for climate models to simulate and study future climate conditions.

Wildfires in the region are characterized by a main summer fire season and by a secondary spring peak that is more evident over the northern regions (Trigo et al 2016). The Iberian Peninsula presents itself as a key region of study in terms of wildland fire adaptation and mitigation plans for the next decades. Indeed, active forest and fire management practices are seen as a tool to mitigate the impacts of climate change in these events. Also, land use management is an important contribute to climate changes adaptation. Nevertheless, such management decisions from authorities and decision makers must be timely informed to be effective. This report intends to present a comprehensive analysis of the impact of climate change on fire risk in Iberia, using a EURO-CORDEX weighted multi-variable multi-model ensemble to estimate both FWI and FWIe. The use of weighted multi-model ensembles in climate studies has been shown to improve climate projections derived from ensembles (Christensen et al 2010, Soares et al 2012, Wenzel et al 2016, Knutti et al 2017, Sanderson et al 2017, Lorenz et al 2018, Eyring et al 2019, Brunner et al 2019, Nogueira et al 2019), allowing to generate more reliable regional climate projections and constrain the uncertainty of climate modelling.

Climate change imposes a formidable strain in companies, institutions, and governments that need to prepare viable and timely adaptation measures to secure the future prosperity of the society. This is true for several sectors such as hydrological balance, droughts, forest fires, agroforestry and sea level rise and coastal erosion, where the uprising of extreme events such as droughts and heatwaves, or extreme precipitation and flash floods, among others, are expected to take a toll in society as it stands. Climate change is also expected to change wildfire regimes and their intensity in several regions around the globe. Past examples already point to this shift, with some of the most destructive and intense fires taking place in Australia, California, or the Amazon Forest in recent years. The Iberian Peninsula, and particularly Portugal, is another relevant example. Situated in a climate change hotspot, in the western tip of the Mediterranean, this region is known for its summer fire occurrences, with several events extensively studied by the scientific community.

In recent years, mainland Portugal was affected by the most intense and destructive fires recorded, such as the 2003 fire season where 300 thousand hectares of forest were burnt, 18 people died, approximately 85 were displaced, and hundreds had to be evacuated from their homes, the referred 2017 fire season that burned more than 500.000 ha, and resulted in more than 100 human lives lost, or the 2018 southern Portugal wildfire, which destroyed dozens of homes and killed thousands of animals. A consequence of these fires was large social, environmental, and economic losses, with the 2017 fire season having a consequent economic cost greater than one thousand million €, the 2018 fire season leaving more than 100 homeless, and the 2022 fire season having a strong impact on biodiversity, natural heritage, tourism, and local producers of Serra da Estrela. Indeed, recent past points towards a “new normal” where frequent extreme fire risk conditions and consequent events take part of everyday life in the warmer months, typically between June and September. This is more worrisome when taking projections of climate change until the end of the 21st century. A recent study showed that summer values of fire risk tend to substantially increase in the future, with a likely stretching of the danger period. The north-western region of Iberia, including the north of Portugal and the north-western-to-central Spain were the regions where larger increases in fire risk in the future were found. These findings are especially noteworthy since these are the regions with more fire-prone vegetation. The same work also points to large differences in fire risk projections among scenarios, calling for a distinct set of adaptation needs that should be timely prepared by stakeholders and authorities. The door to climate change adaptation is thus opened, and it is now time for companies, institutions, and governments to make an effort at preparing and adopting new strategies and policies. Hence, a new research project within the framework of the National Roadmap for Adaptation 2100 - Portuguese Territorial Climate Change Vulnerability Assessment for XXI Century (RNA 2100), was born. The project pillar objectives include the development and definition of adaptation strategies for Portugal and the development of storylines, where the choice of climate models, multi-model ensemble, and regionalization are key components, and where adaptation strategies to wildfires resulting from climate change is an important achievement.

To the best of our knowledge, there is still no comprehensive analysis of the relationship between atmospheric instability and wildfire danger indices. The first goal of this report is to produce a climatological characterization of CHI, FWI and FWIe over IP based on state-of-the-art reanalysis ERA5 data provided by the European Centre for Medium-Range Weather Forecasts (ECMWF). Then, this report focuses on the large fire events that took place in 2003, 2017, and 2018 in Portugal and for each event, performances of FWI and FWIe are compared. This analysis allows assessing the usefulness of FWIe in regions and during periods where atmospheric instability plays a decisive role in the development of wildfires contributing to a more efficient deployment of suppression activities. This is the first study expanding FWI with projections of atmospheric instability into the future, a critical component of wildfires usually not taken into consideration. Additionally, the current report is the first to consider a weighted multi-model ensemble built over a multi-variable quality analysis spanning the three Representative Concentration Pathways (RCP) emission scenarios (see WP2). The report's key objective is to strengthen the understanding on how fire risk in the Iberian Peninsula is projected to change in the future by taking advantage of a state-of-the-art index such as the enhanced FWIe and considering the three RCPs. To accomplish that, two specific objectives were pursued: (1) Computing FWI and FWIe using the output of a set of EURO-CORDEX RCM simulations downscaled from different GCMs for the historical and for three future periods under three emission scenarios: RCP2.6, RCP4.5, and RCP8.5; and (2) estimating the number of days in each period with FWI larger than the 90th percentile. The anomaly in the number of days obtained in the future and on historical periods is estimated for a weighted multi-model ensemble of FWI and FWIe, and the differences between the two are analysed.

This analysis allows to provide a clear insight on how atmospheric instability may change the evolution of fire risk extremes when comparing with the original surface-based fire weather index. Finally, this report aims at producing the needed fire risk information to assist decision-makers on the different adaptation needs associated with the diverse mitigation targets.

Although FWI may be an important asset to develop climate change adaptation strategies and policies, the fire risk is not equivalent to having a fire per se. Furthermore, having high values of risk and relatively small fires is not fundamental for adaptation, since the key wildfires are those with very high energy, which need strong operational actions, tend to burn for several days, and are characterized by large burnt areas. A recent work by DaCamara et al developed a method that allows to generate synthetic values of Fire Radiative Power (FRP; a measure of heat output from a fire related to how quickly fuel is being consumed) from FWI by using a model that consists of a truncated lognormal central body with Generalized Pareto distributions as tails and using FWI as a covariate. By taking advantage of this model, it is possible for the first time to project probabilities of wildfire activity for climate change scenarios using FWIs from RCMs. This allows for a jump forward in the study of probabilities of wildfire activity into the 21st century, which until now was focused on fire risk indices directly obtained from meteorological variables. This work aims at performing this jump forward, by using EURO-CORDEX RCMs to estimate FWI for an historical period and for different projected scenarios encompassing the 21st century, namely RCP2.6, RCP4.5, and RCP8.5; and then to generate synthetic values of FRP using the method described in DaCamara el al. This work attempts to answer to the question: what is the expected future change in the probability of having large fires in mainland Portugal due to climate change and how is this change driven by the different greenhouse gas (GHG) mitigation pathways over the century? This work attempts at answering this main topic by taking advantage of an ensemble of regional climate models from the EURO-CORDEX initiative, observations of Fire Radiative Power (FRP) from the Moderate Resolution Imaging Spectroradiometer (MODIS).

2. Data and Methods

2.1. Study Region

The current report is focused on the Iberian Peninsula, and the regionalization described in Trigo et al (2016) is adapted here. The authors used the burned area associated to 66 autonomous regions (AR) in Portugal and Spain and normalized it by each AR area to obtain the normalized burned area. Then, a cluster analysis, using the K-means algorithm, was applied to the Normalized Burned Area (NBA) of the 66 ARs, and finally retained four statistically significant clusters (Figure 1). These include a north-western cluster aggregating the northern half of Portugal and the extreme northwest of Spain (NW), a south-western cluster including the southern and interior regions of Portugal and central and south-western Spain (SW), an eastern cluster including the coast and pre-coastal areas east of Gibraltar until the Pyrenees (E), and a northern cluster corresponding to regions over the mountainous sectors of northern Spain, such as the Asturias, Calabria, and Basque Country (N) (Figure 1).

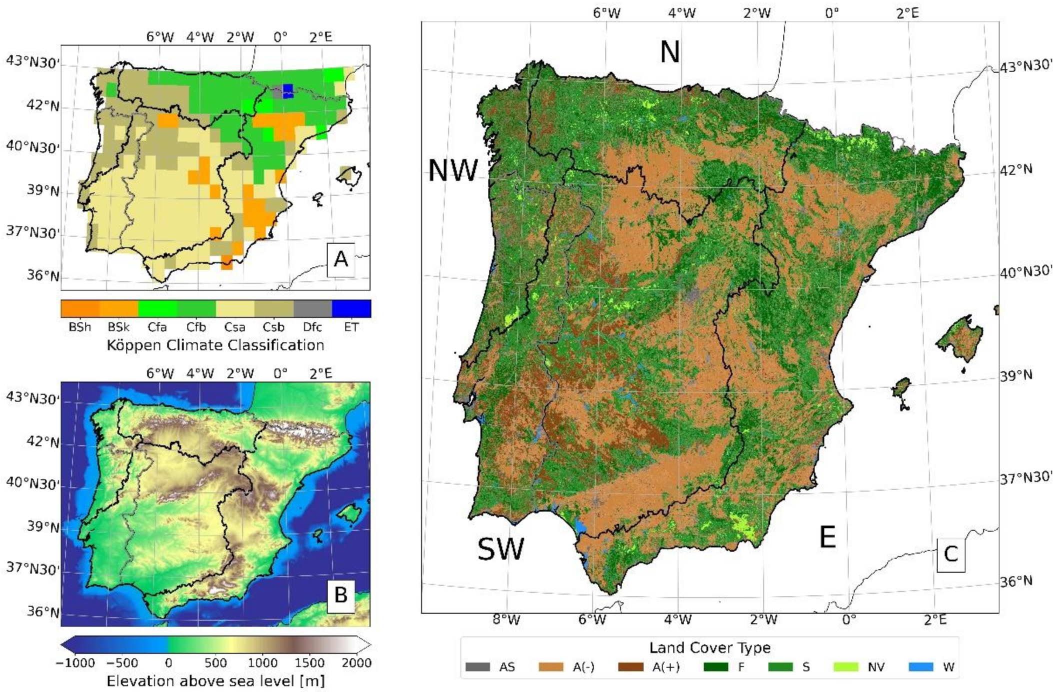

Figure 1 – Detailed view of the study region that includes the (A) Climate Köppen Types as follows: BSh – Hot semi-arid; BSk – Cold semi-arid; Cfa – Humid subtropical; Cfb – Temperate oceanic; Csa – Hot summer Mediterranean; Csb – Warm summer Mediterranean; Dfc – Subarctic; Et – Tundra; (B) topography, and (C) land cover types labelled as follow: AS – Artificial Surfaces; A(-) – Agricultural (less forested); A(+) – Agricultural (more forested); F – Forest; S – Shrub; NV – No vegetation; W - Water. In each subplot the clusters were drawn (in black) as well as the borders (in grey) of Portugal and Spain.

The study region comprises the Iberian Peninsula and is shown in Figure 1, where the Climate Köppen Types (Figure 1A), topography (Figure 1B), and land cover types (Figure 1C) are detailed. The Climate

Köppen Types (Figure 1A) showing that the IP mainly presents hot or warm Mediterranean summers while the north-eastern area is mostly temperate all year long. The topography of the study region (Figure 1B) shows most of southwestern Iberia being flat presenting low values of altitude whereas central, eastern, north, and north-eastern Iberia include large mountain ranges, peaking at nearly 3500m with most areas being below 1000m. Land Cover Types were retrieved from the Copernicus Land Monitoring Service, CORINE Land Cover (CLC) 2018, derived from satellite imagery obtained at different times of 2017 (e.g. forest types were retrieved during the July-August period since this land cover is more developed at this time of the year), with an approximate resolution of 100m. The spatial distribution of land cover types reveals a close connection to topography, with agricultural covering much of the mountainous slopes and river valleys of the Peninsula. In the main mountain ranges located in the central and north-western sectors of the Peninsula, there is a prevalence of forested areas. In central Portugal, a scar of no vegetation is visible for which the 2017 summer wildfires contributed substantially, however the October wildfires are not visible due to the time of retrieval for this land cover type (July-August).

2.2. Reanalysis data

Surface and atmospheric data were retrieved from the 5th generation of the European Centre for Medium Range Weather Forecasts (ECMWF) global reanalysis (ERA5), available in a 0.25° x 0.25° spatial grid, to calculate CHI, FWI, and FWIe. For the computation of these indices, we retrieved relative humidity (RH) at 850-hPa, temperature at 2m, 700- and 850-hPa, dew point temperature at 2 m, U and V wind components at 10m, and accumulated daily precipitation (computed from hourly values). All fields refer to 12 UTC.

2.3. EURO-CORDEX model data

The EURO-CORDEX high-resolution simulations were performed under the CORDEX effort (Jacob et al 2014, 2020) and provide a larger number of regional climate runs over a common domain. The runs here considered were produced with a grid of 0.11° horizontal resolution, dynamically downscaling the original CMIP5 GCM ensemble. Current climate simulations of EURO-CORDEX ran from 2006 onwards following different future scenarios of anthropogenic forcings: RCP2.6, RCP4.5, and RCP8.5. In this study, three projected periods were used and are referred as “future periods” onwards (namely, the begin-century 2011 – 2040, the mid-century 2041 – 2070, and the end-century 2071 – 2100). On the other hand, the historical period for these regional climate models was simulated from 1950 until 2005 following historical emissions. Hence, for this study the period 1971 – 2000 was selected as the historical period. It is worth noticing that the simulations are not synchronized in time due to GCMs forcing. These RCPs are defined according to the correspondent effect of greenhouse gas emissions in the radiative forcing values in 2100, which are +2.6, +4.5 and +8.5 Wm-2 relative to pre-industrial era. Hence, the most mitigated scenario is the RCP2.6 and the less mitigated one is the RCP8.5. While in the former, the peak of global annual greenhouse gas emissions occurs between 2010 and 2020, for the latter the emissions grow continuously throughout the 21st century. Finally, the emissions of RCP4.5 peak around 2040 and lessen afterwards (Moss et al 2010, Riahi et al 2011; van Vuuren et al 2011).

As described in WP2, from the full set of EURO-CORDEX RCM simulations available in the Earth System Grid Federation (ESFG) data portal, 13 sets were selected (historical/future) to be run for the historical and future scenarios and the 3 RCP emission scenarios (Table 1). Both fire risk indices FWI and FWIe were computed for the 13-model ensemble.

Table 1 – EURO-CORDEX RCMs used in this study, along with the responsible institute and the forcing GCMs. The 13 simulations have historical, RCP2.6, RCP4.5, and RCP8.5 scenarios (see WP2).

RCM	Institute	GCM
CCLM4-8-17	CLM	EC-Earth
ALADIN63	CNRM	CNRM-CM5
HIRHAM5	DMI	EC-Earth HadGem2-ES
REMO2015	GERICS	NorESM1-M
RACMO22E	KNMI	CNRM-CM5 EC-Earth HadGem2-ES
REMO2009	MPI	MPI-ESM-LR
RCA4	SMHI	EC-Earth HadGem2-ES MPI-ESM-LR NorESM1-M

In this report, a new multi-variable approach to build a multi-model ensemble was used to assess future meteorological fire risk conditions, using two fire weather indices (FWI and FWIe). Since both indices need multi-variable information, this new approach is key to preserve the physical consistency among climate projections. An evaluation of the ability of 13 RCMs from EURO-CORDEX in reproducing precipitation, maximum and minimum temperature was assessed against the Iberia01 observational gridded dataset (Herrera et al 2019). This validation was performed in Lima et al (2023), and is described in detail in WP2, considering a set of error metrics (mean bias, mean absolute error, root mean squared error, standard deviation, correlation, Willmott-D Score, Perkins skill score, and Yule-Kendall skewness) for the historical period (1971-2000) over the Iberian Peninsula. For each model and variable, the weights were obtained considering the individual model's performance in representing the observed climate. For the final weights of each model considering the multi-variable performance, a final weight is computed where precipitation corresponds to 50% and maximum and minimum temperature contributes 25% each one. The weighted multi-variable multi-model ensemble reproduced well the precipitation and temperature patterns over Iberian Peninsula when compared with the Iberia01 dataset (Lima et al, in review), which give us confidence on using this approach for this study. Finally, the multi-model ensemble is computed with those weights, giving physical consistency to the assessment of meteorological fire risk based on FWI and FWIe.

The list of daily meteorological variables needed for the development of this study include maximum and minimum 2-m temperature, surface pressure, specific humidity, daily accumulated precipitation, 10-m wind speed, 850 hPa and 500 hPa temperature, and 850 hPa specific humidity. Relative humidity is obtained from specific humidity, 2-m mean temperature is the simple average between maximum and minimum temperatures, the 700 hPa temperature was estimated by interpolating between 850 hPa and 500 hPa temperatures, and dew-point temperature at 850 hPa was computed from 850 hPa specific humidity.

2.4. Continuous Haines Index (CHI)

It was used reasonable atmospheric levels to evaluate the CHI considering the average topography of the IP. Thus, it was chosen to use 850 - 700 hPa. The CHI is defined as:

$$CA = (T_{850}-T_{700})/2 - 2 \tag{1}$$

$$\begin{gathered} CB = \min(T_{850}-Td_{850}, 30)/3 - 1 \\ \text{If } CB > 5\text{, then: } CB = 5 + (CB-5)/2 \end{gathered} \tag{2}$$

$$CHI = CA + CB \tag{3}$$

where T700 and T850 are the absolute temperature values at 700- and 850-hPa, respectively, and Td850 is the dew-point temperature at 850-hPa. The min (T850 − Td850, 30) term in equation (2) indicates that an upper bound of 30° C was defined for the difference between the temperature and dew-point temperature at 850 hPa. Dew-point temperature (Td) was computed from T and RH according to the Magnus formula, which yields a conversion between relative humidity and dew-point temperature with a relative error lower than 0.4% over the range -40° C ≤ T ≤ 50° C. Daily values of CHI for the IP spanning the study period of 1980-2020 were computed according to relations (1)-(3) using reanalysis data from ERA5.

2.5. Fire Weather Indices

The CFFWIS components were estimated following the procedure described by Van Wagner (1987), namely the Drought Code (DC), Duff Moisture Code (DMC), Fine Fuel Moisture Code (FFMC), Initial Spread Index (ISI), Build-up Index (BUI), and the Fire Weather Index (FWI). The first three have a memory component and are denominated the fuel moisture codes, based on consecutive daily observations of 2-m temperature, relative humidity, 10-m wind speed, and 24-hour accumulated precipitation. The remaining three are the fire behaviour indices. Originally the indices are to be calculated at noon, however EURO-CORDEX only provides daily values of the variables needed. Hence, following other studies (Moriondo et al 2006, Giannakopoulos et al 2009, Carvalho et al 2009), it was computed the CFFWIS components based on daily mean 2-m temperature, relative humidity, and 10-m wind speed, and daily accumulated precipitation. Thus, FWI values (and therefore the other CFFWIS indices) are estimated on a daily basis for each grid-point of each individual model for the historical and future periods (over three different emission pathways).

It was also computed FWIe (Pinto et al 2020) that incorporates the Continuous Haines Index (CHI), which was designed to evaluate atmospheric instability (Haines 1988) that promotes convective fires (Mills and McCaw 2010). CHI is defined by an instability term (CA) based in the difference between temperature at 850 (T850) and 700 hPa (T700), and by a moisture term (CB) based on the difference between temperature (T850) and dew point (DP850) at the lower level (850 hPa). The CHI is estimated for each grid cell of each model for the historical and future periods. Then, the FWIe is estimated as a function of FWI and CHI, calibrated so that the probability of exceedance of a pre-defined threshold of released energy on a Generalized Pareto dependent on FWI is identical to the one given by the more complex Generalized Pareto model dependent on both FWI and CHI. A comprehensive explanation and validation of the FWIe methodology can be found in Pinto et al. (2020).

A validation of FWI estimated with EURO-CORDEX regional models against FWI estimated with the fifth generation of the ECMWF atmospheric reanalysis ERA5 (Hersbach et al 2019) was firstly undertaken. The reanalysis was used instead of observations due to the lack of some of the observed variables needed to compute FWI and FWIe in the region. The models' ability to reproduce the observed probability distribution functions (PDFs) was quantified by the Perkins skill score (S) (Perkins et al 2007). This score provides a measure of similarity between the simulated and observed empirical PDFs, with S=100% if the model perfectly reproduces the observed empirical PDFs. Two different methods were used to estimate the S score. The first for the full PDF (the so-called S score), and the second for the average between two sections following (Boberg et al 2009), where the first section comprises the data until the 90th percentile and the second from the 90th percentile onwards (the so-called S90 score). This comparison will ensure that the multi-model ensemble is able to reproduce the observed (here reanalysed) distributions.

2.6. On the comparison between reanalysed FWI, FWIe, and CHI

For the 41 years of this study (1980-2020), a series of climatological fields were produced for each variable over the study region for the period spanning from June to September, hereafter referred to as summer months. Climatologies for the whole year and for an extended period of colder months (November-April) may also be found in the supplementary material. Additionally, the intra-annual evolution of each index is presented in the form of boxplots, considering the clusters described in subsection 2.1, where the box indicates the interquartile distance, the dash inside the box indicates the median and the whiskers represent the 5th and 95th percentiles.

Changes of CHI, FWI, and FWIe in the past decades were assessed based on the seasonal variability that was analysed considering the past four decades independently. Additionally, the same distributions for each cluster individually were produced. Spatial change was assessed by computing the long-term trend for each of the variables using a monotonic seasonal Mann-Kendall trend test for the summer months. This trend was shown as an average index change per decade and the non-significant areas (5% significant level) were identified.

The two fire risk indices were compared with the observed FRPs over the IP, with the objective of crossing risk with occurrences. FWI and FRP are stratified into predefined classes according to the following criteria: for FWI, the danger class system detailed in EFFIS, which presents the indices in 6 classes from “Very low” to “Extreme” danger; and the FRP, percentile-based classes as defined by percentiles 10, 33, 50, 67 and 90 of FRP relative to the IP. For each of the FRP classes, a comparison was made between the FWI and FWIe associated with fire events. For this purpose, a linear regression was estimated for each FWI class (totalling 6 equations), the slope of each regression indicating which index has the largest magnitude. Furthermore, for each FRP class a Kernel Density Estimation (KDE) plot was obtained from the sample, using a Gaussian kernel. For both the linear regressions and the KDE plot, the FRP values were used as weights for the computations, i.e., the larger the FRP absolute value the larger the influence on the result when comparing with other elements in the same set.

Furthermore, we also analysed case studies, the two fire episodes of June and October 2017, and the two Monchique episodes of 2003 and 2018. The first case, in 2017, was chosen as a validation of the applied methodology to compute the indexes as previous studies are available. The fire season of 2017 was exceptional for central and northern Portugal and parts of Galicia, although only the region inside the borders of Portugal and north of the 39.1° N parallel were analysed in this study; this area encompassed

73% of all occurrences at that time and saw an excess burning of 500 000 ha and the tragic passing of 116 people. Two additional case studies were conducted where, instead of the whole fire season, only consecutive days of great fires over a small area were analysed. The fire season of 2003 was outstanding for western Europe and particularly for Portugal with a massive fire that affected the Algarve, in the Monchique region. Years later, in 2018, 80% of the same burned area in Algarve was again affected by a large fire. The study area of Monchique was chosen because of the large mountain range in the area, increasing the interest regarding interactions with atmospheric instability. In all cases, a daily analysis was performed by taking the values of each variable and the respective daily FRP. Besides computing the absolute values of these variables, it was also considered their anomalous character, using standardized anomalies, i.e., the number of standard deviations above/below the climatological value for the region and for that period. Additionally, it was also computed the associated probability of exceedance, assuming that the distribution of these values was normal.

2.7. On the future extreme FWI and FWIe days

To evaluate the change in the number of days with high fire risk in the future it was selected the 90th percentile as the daily threshold of FWI and FWIe for each grid cell. The number of days per year in the extended summer (June to September) with FWI and FWIe above this threshold are totalled. By definition, for the historical period, there are about 12 days above the 90th percentile by pixel (there are 122 days in June, July, August, and September - JJAS). Then, the difference between the 30-year mean of exceedance days in the future and historical periods is estimated, i.e., the climatological anomaly of number of extreme FWI days. The 90th percentile is computed over the historical period based on a methodology that avoids artificial discontinuities at the beginning and the end of the base period percentile time-series (Zhang et al 2005). The historical percentile is obtained for FWI and FWIe on a daily basis using a 5-day moving-window. The percentile based FWI and FWIe minimize the impact of biases on the results since each threshold is set for each grid point and model.

2.8. On the projections of Fire Radiative Power (FRP) and return periods of burnt areas

Here, Fire radiative power (FRP) was obtained based on the Moderate Resolution Imaging Spectroradiometer (MODIS) instrument aboard the Terra and satellites, specifically from MODIS Collection 6 Active Fire Product (Giglio et al., 2020). The data consists of 63,942 hotspots over continental Portugal with the location, calendar date, occurrence time, and FRP estimates spanning the 20-year period encompassing the years 2001 – 2020.

By taking advantage of the base model with FWI as covariate developed by DaCamara et al, log10(FRP) are synthetically generated for the bias corrected 13-model historical and projected scenarios. Then, results are to be analysed by means of cumulative distribution functions (CDFs). The exceedance ratio is then estimated: the probability of exceeding a given log10(FRP) in the future is compared with the same for the historical, which gives the number of times a probability of exceedance is projected to occur. Final results are presented for the weighted multi-model ensemble.

The return periods of burnt area are estimated by taking advantage of a model with yearly cumulative daily severity rating (CDSR) and annual burnt area as covariates.

3. Results

3.1. Past climatological analysis

In the summer months of June, July, August, and September (JJAS) it is possible to identify higher values of CHI in the southern part of Iberia, namely in the southeast/central-east regions (Figure 2A), with a noticeable band in the 3° W meridian, which roughly corresponds to the junction of the Baetic Mountains, the Central System, and the Iberian System all visible in the topographic map (Figure 1B). Spatial patterns of FWI (Figure 2B) show the largest values located over central Iberia, an area of typical Mediterranean climate (Figure 1A), with hot to very hot and dry summers. Regions characterised by larger FWI values are typically contained inside the SW and E clusters. Finally, the spatial climatological pattern of FWIe (Figure 2C) is overall more similar to the one of FWI, as expected since these variables are directly related. Nevertheless, the peak of CHI values observed in the border separating SW and E clusters (Figure 2A) is partially recognizable in the FWIe (Figure 2C) but less evident in the original FWI pattern (Figure 2B). Spatial patterns of CHI, FWI, and FWIe representing yearly and winter (DJF) climatologies may be found in supplementary material Figure S1A – F, with similar results when considering the yearly patterns and noticeably lower values in winter.

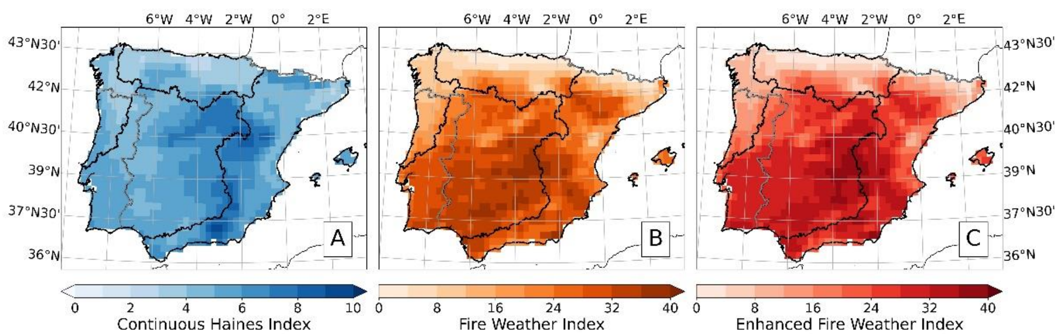

Figure 2 – Field climatologies for the Iberian Peninsula for the 1980-2020 period considering the summer months of June, July, August, and September (JJAS), for the three indexes (A) CHI, (B) FWI and (C) FWIe.

The annual cycle of the three indices is displayed in the form of monthly boxplots in Figure 3, for each spatial cluster. The annual cycles depend on the region of analysis, conditioned by the different types of climates, topography and land cover, as depicted in Figure 1. The CHI distribution has the most notable change from region to region since the seasonal amplitude varies dramatically (Figure 3A-D). The northern part of Iberia, i.e., NW and N clusters (Figures 3B and 3C, respectively), shows lower overall values of CHI (around 3 in winter and nearly 4 in the summer), comprising the more humid areas of the Peninsula, and present a lower yearly amplitude. In turn, the drier and warmer southern and central areas, i.e., SW and E clusters (Figures 3A and 3D, respectively), show the largest amplitude from winter to summer, and the largest values of CHI, surpassing 6. Additionally, the E cluster (Figure 3D) presents the greatest variability, namely in the warmer months. This higher variability found in the E cluster may be due to the large meridional extent of the cluster, comprising regions from coastal to inland both in Southern Spain and bordering the Pyrenees.

FWI, in comparison with FWIe, has a more well-defined seasonality, with higher values and variability in the summer months (Figures 3A–D), maximum median values around 35 and 95th percentile maximums reaching 45. The SW cluster (Figure 3A) is characterized by a demarked annual cycle of FWI, with higher values in summer and low variability overall. Moreover, the variability of FWI in the E region can be explained by having its southernmost area sharing the characteristics of the SW cluster (higher FWIs in warmer months) while the northern area has a temperate oceanic climate (Figure 1A), with milder summers and winters (less seasonal temperature variation), contributing to year-round lower FWI. The NW and N clusters (Figures 3B and 3C, respectively) have lower FWIs when compared to SW and E – with median values of 15 and 10, respectively – with the NW region having a mostly warm-summer Mediterranean climate and the N region, with a mountainous character due to the presence of the Cantabrian Mountains (Figure 1B), having a mix of that climate type with temperate oceanic climate (Figure 1A). The annual cycles of FWIe (Figures 3A–D) show a similar behaviour to those of FWI across all regions, usually with lower average and spread values, excepting for July and August in the E region (Figure 3D), where the variability increased overall. It is also noteworthy to say that different areas within these clusters present different medians and respective extremes, due to smaller scale different land cover and climate types.

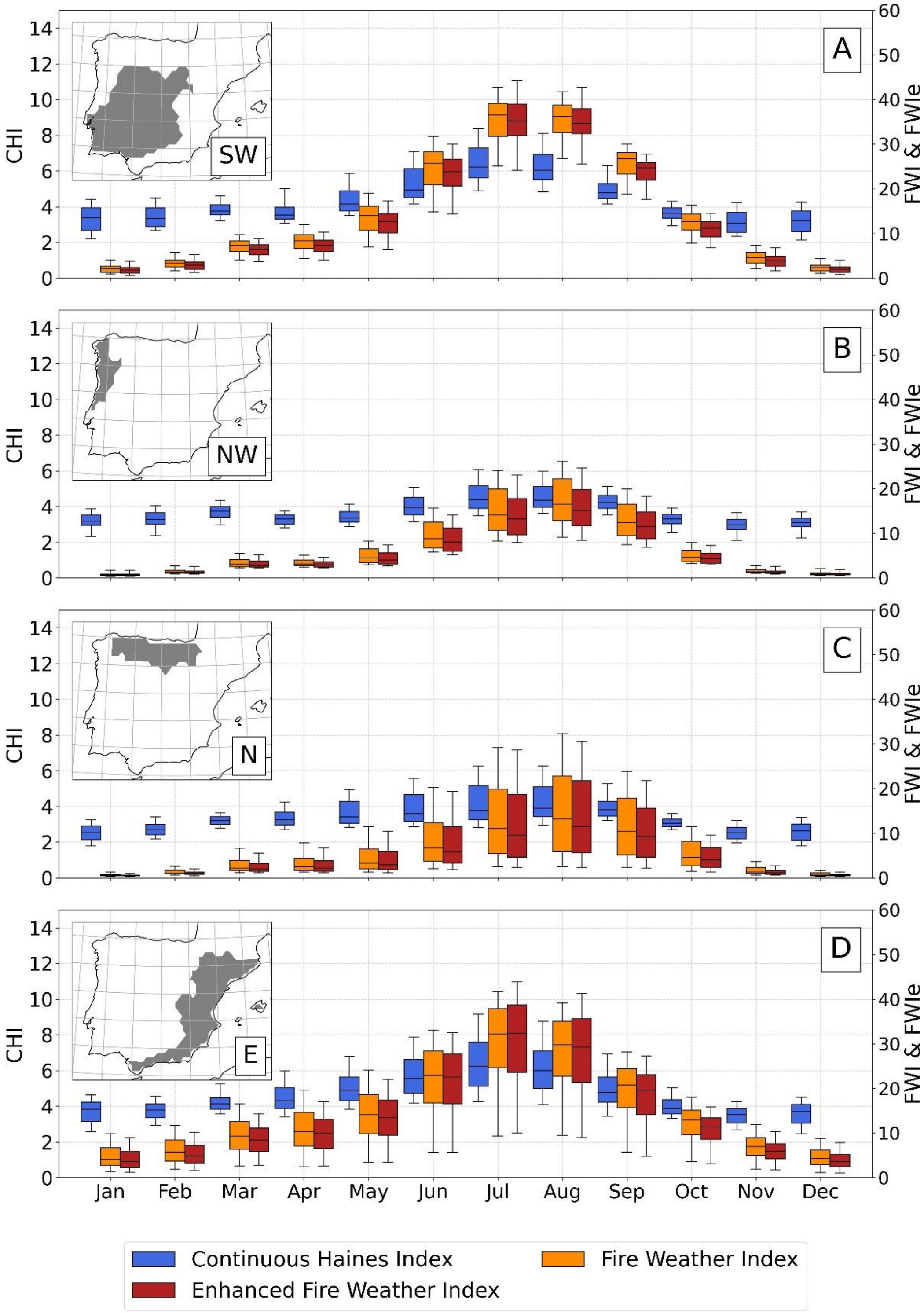

Figure 3 – Annual cycles for each of the 4 clusters during 1980-2020, for CHI (blue boxes), FWI (orange boxes) and FWIe (red boxes). The scale for CHI is on the left y-axis, and the scale for FWI and FWIe is on the right y-axis.

3.2. Past decadal evolution

Long-term changes were evaluated by performing a decadal evolution assessment of the IP average of CHI, FWI and FWIe fields (Figure 4). From the decadal evolution of CHI (Figure 4A), a similar seasonal cycle as seen in Figure 3 may be noticed, with median values of around 3 in the colder months and exceeding 6 from June to August. Overall, the months of November, December, and January show nearly no decadal changes, while from February to April there has been a slight decrease since the 2000s decade. However, from May to August it can be observed a general increase since the 1990s, which can be also found in September and October since the 2000s (Figure 4A). It was performed a similar assessment on a regional basis and the main conclusions described above for the whole IP are also visible when considering SW and E regions (Figures S2A and S5A, respectively), and to a lesser degree NW and N regions (Figures S3A and S4A). The spatial distribution of long-term CHI trends is presented in Figure 5A confirming the identified increments, where the greatest change in CHI appears to be mainly located in the southeastern region of IP with increases of approximately 0.25 and 0.26 per decade, in regions SW and E, respectively (supplementary material Table S1 fully describes changes per decade and statistical significance). Regions NW and N show smaller increases of about 0.06 and 0.15 per decade, respectively, with only 49% and 66% of their areas presenting statistically significant changes.

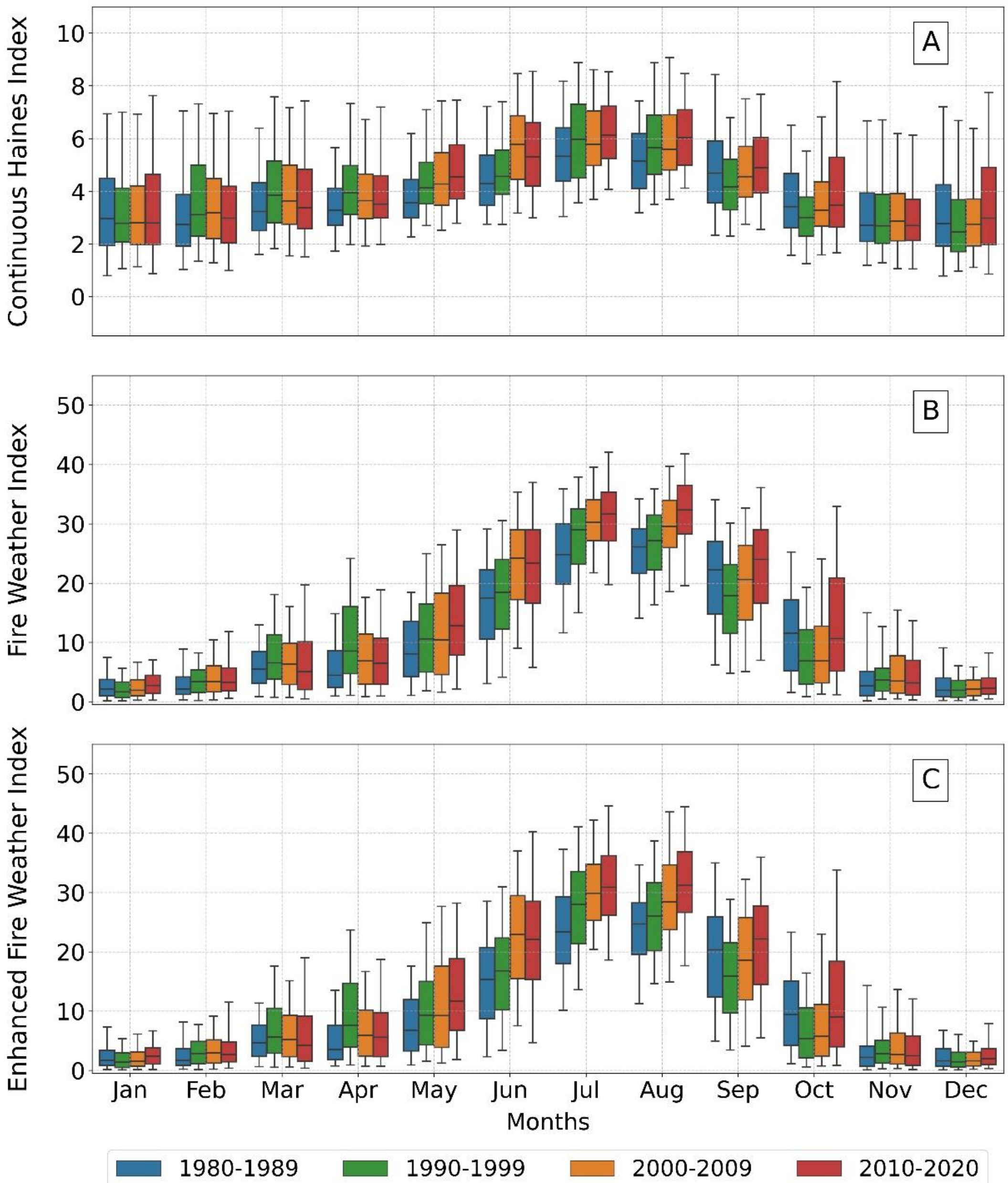

Figure 4 – Boxplots showing evolution of the yearly distribution in the IP average throughout the decades in the 1980-2020 period for the variables (A) CHI; (B) FWI; and (C) FWIe.

Decadal evolution of IP average values of FWI and FWIe (Figures 4B and 4C, respectively) show similar behaviours as observed in seasonal distributions of the SW and E regions (Figures 3A and 3D). As with CHI, colder months (in this case, from November to February) do not show substantial changes both in FWI and FWIe, while in March and April there is slight decrease since the 2000s. On the other hand, when considering the summer months there is a general major increase, namely in May, June, July, and August. Conversely to CHI, these increases affect all regions (Figures S2-5B and S2-5C), with special relevance in regions SW and E. As with CHI, the larger trends are located towards the southeast of the Peninsula (Figures

5B and 5C), with almost all the IP presenting statistically significant positive trends. Figure 5C shows, for the FWIe, an extended region where the positive trends exceed 4 average index change per decade, which results from the combined increases in both CHI and FWI around the same approximated areas. SW and E are the regions showing most relevant changes regarding these decadal trends with most of them having significant grid boxes with large positive values. The SW region shows 100 % of its territory with statistical significance and an average increase of approximately 1.9 and 2.2 per decade for FWI and FWIe, respectively, while the E region shows slightly lower increases of circa 1.9 and 2.1 for the same variables (Table S1).

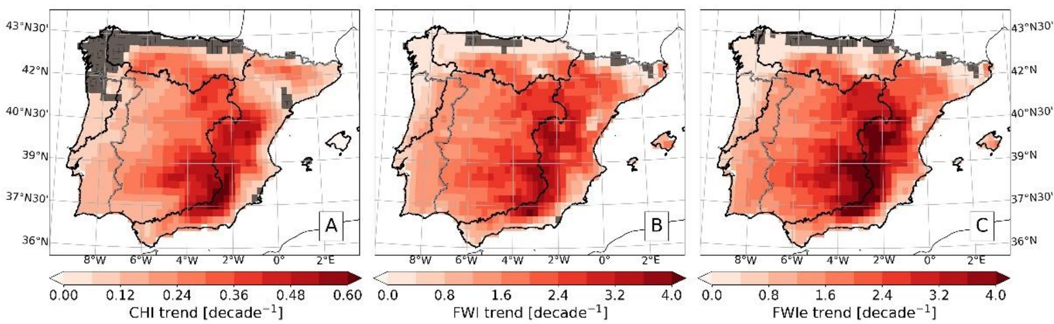

Figure 5 – Long-term trend for (A) CHI, (B) FWI, and (C) FWIe, considering only summer months (June to September), for the 1980-2020 period. Computed from a monotonic seasonal Mann-Kendall trend test. Grey shaded areas show pixels where trends are not significant at the 5% statistical level. Trends are shown as the average index change per decade.

3.3. Past fire occurrences and FWI vs FWIe

The relationship between real fire occurrences was examined using FRP as a measure of power released by each fire observation. The classes of FRP, that were defined according to the values of percentiles 10, 33, 50, 66 and 90, respectively 24.9, 53.6, 81.4, 130.1 and 362.3 MW, were aggregated. Each panel of Figure 6 presents the relationship between the FWI and FWIe in two different ways: (1) by means of KDE plots as shown in a grey scale, and (2) by means of linear regressions as shown by coloured lines, estimated for each FWI class (shown as vertical black bars).

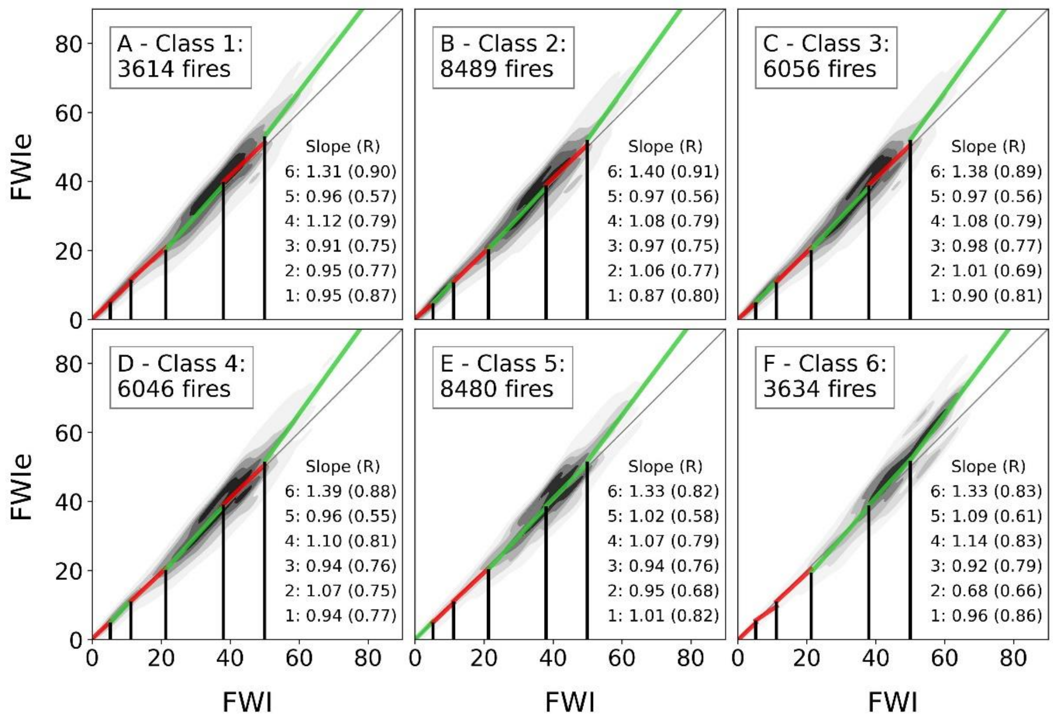

Figure 6 – Comparison between real FRP observations (from 2001-2020, considering the whole IP) and the FWI and FWIe values for the same occurrence. Both FRP and fire danger indexes were divided into discrete divisions: FRP based on the percentiles 10, 33, 50, 67 and 90 of all occurrences (A-F panels, with respective number of FRP's in that division); and the FWI was divided according to the Fire Danger Classes provided by EFFIS (vertical black lines). Linear regression for each FWI class compared to FWIe is shown in coloured lines: red (green) for slope exceeding (subceeding) the identity line. Values of slope and associated Pearson R values are shown in each panel, with ascending values (1-6) corresponding to the increasing FWI classes (bottom left to top right within each individual subplot).

It is immediately noticeable through the KDE plot that the bigger the occurrence (i.e., bigger the class of FRP) the more likely the event to happen during more extreme values of FWI. Fires with FRP within the first four classes (Figures 6A-D), with FRP lower than 130.1, were more likely to coincide with "high danger" FWIs class (up to the fourth vertical black line, in Figures 6A-D), with these classes having upwards of 35% of their observations inside this FWI class. However, fires with FRPs larger than 130.1 have a maximum representation in the "very high danger" FWI class (above the fourth vertical black line, in Figures 6E-F), both also having upwards of 35% representation in this class. It is worth noticing that fires with the greatest FRP values (Figure 6F) happened more frequently during the "extreme" than "high danger" FWI class (30% of the total number of the largest FRP occurrences compared to 25.3%), showing a complete shift in danger associated with the largest fires compared to small FRP classes.

Looking closely at each FWI class for every panel (coloured lines), the linear regression is presented with the associated slope (numerically and in colour) and Pearson R value. The first noticeable thing is the FWI classes that preserve the slope type when comparing the diverse panels. Firstly, the middle FWI classes (“moderate” and “high”, 3rd and 4th ones respectively) show the same behaviour in all panels, with the “moderate” (“high”) class having a slope below (above) that of the identity line - averaging 0.94 (1.10) -, meaning the FWIe classifies the same FRP with a lower (higher) value respective to the FWI. This demeanour points to the different nature of FWIe, favouring a larger danger index for higher FRP values in the upper middle classes. Adding to this, the “extreme” (6th) FWI class consistently presents higher FWIe values, seen in all FRP classes, with the highest R values, upwards of 0.83. The reverse can be verified in the “very low” (1st) FWI class, with exception for the 5th (Figure 6E) FRP class. Additionally, the “very high” (5th) FWI class presents slopes below the identity line in the first four FRP classes (Figures 6A-D) while the last two are above (Figures 6E-F) thus, higher (lower) FRP observations are better rep-resented by higher values of FWIe (FWI). Concluding, Figure 6 overall shows that higher FRP (i.e., more intense fires) tend to logically occur in higher FWI values and the FWIe generally increases the meteorological danger in these occurrences while in lower FWI classes, this index remains with greater values compared to the FWIe.

3.4. Past case studies

Figure 7 aggregates the information regarding CHI, FWI, FWIe and FRP during the 2017 extended fire season in Portugal, as well as the shapes of all identified burned areas. For the first episode, on June 17th, the CHI reached a value of nearly 10, an extreme value with a probability of exceedance of around 2.5%, which propelled the increase in the FWIe in respect to the FWI, with the latter having a value exceeding 30 and the former reaching 40, which is close to the 2.5% probability of exceedance (Figure 7B). This episode, as evidenced by the grey bars (representing the natural logarithm of FRP) in Figure 7A, had one of the highest FRP values of this fire season, while the affected area was quite large, as evidenced by Figure 7C (in red). The October 15th episode, towards the end of the extended fire season, shows the recorded maximum FWI values for this region, with a probability of exceedance on the order of 0.005% (Figure 7B). During this episode, as already mentioned, CHI was also very high, with values resembling those of June (~10, probability of exceedance of 2.5%), however in this instance, the increment given to the FWIe in respect to FWI was not so relevant since the later was already a record value in itself. This episode led by far to the largest burned area, as seen in Figure 7C (in purple), with several major scars (several larger than 20 000 ha) located all over central and northern Portugal. Comparing both episodes, it becomes apparent that the June event suffered a greater influence from atmospheric instability, as mentioned in Pinto et al. [2020] and depicted in Figure 7, while this contribution was relatively lower in the October episode. These results reinforce the idea that looking at the atmospheric instability, as well as the associated meteorological fire danger, can provide more insightful information to better characterize extreme events.

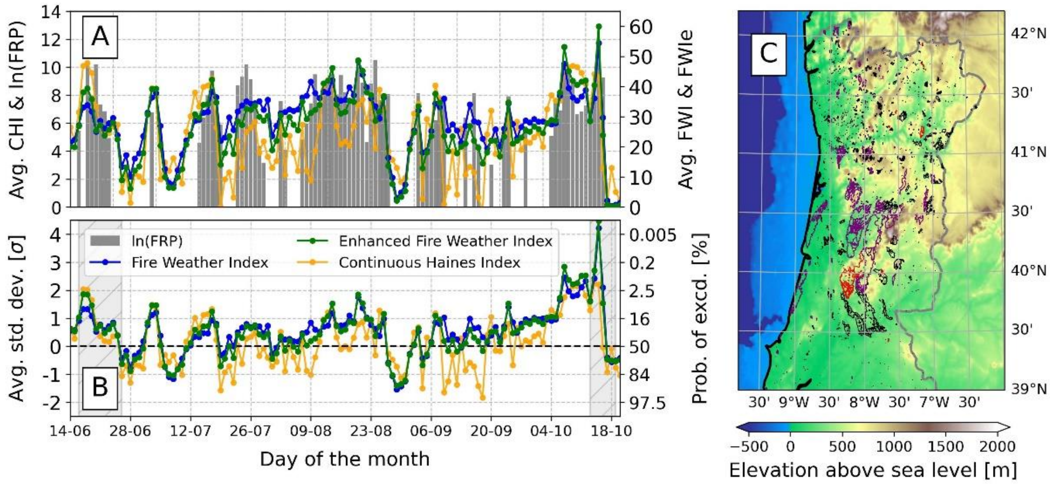

Figure 7 – Comparison of the evolution of the CHI (yellow), FWI (blue) and the resulting FWIe (green) during the Portuguese 2017 fire season. (A) shows the daily average of each variable spatially averaged over the affected areas in Portugal, and the natural logarithm of the daily FRP sum in grey bars. (B) shows the exceedance over (or under) the mean value of each variable in the number of standard deviations, and the approximate probability of exceedance can be seen on the right. Shaded grey areas represent the two time periods of study mentioned in the text and are shown in (C) with respective affected areas in different colors (red for 16/06-25/06 and purple for 13/10-18/10). More details can be found in the methods subsection.

The two Monchique study cases considered here are shown in Figure 8, in the top panel (Figure 8A) the location of these events in the southwestern IP region of Algarve, Portugal, is presented. The two-coloured shapes outline the two burned areas for 2003 (larger one, in purple) and 2018 (smaller one, in red). Additionally, the topography of the area, which is presented as a colour map, shows that the affected region was mostly over a mountainous region, topping at roughly 900 m but with several peaks reaching 600 m. This area is mostly composed of warm summer Mediterranean climate, generally with mild wet winters (Figure 1A), and with a land cover composed mostly of shrubs and forest (Figure 1C). Middle and bottom panels (Figures 8B-C) show the cases for August 2003 and August 2018, respectively, showing the absolute values, the associated excess standard deviation and probability of exceedance for all indexes. However, these cases only show the period corresponding to the large fires in the region, shown in Figures 8B3 and 8C3 as both the individual FRP observations (coloured scatters, according to time of occurrence) and the burned area captured in latter reports (in grey shade, Figure 8B3 does have regions with no FRP shown inside the shape since it occurred later in the season).

The August 2003 Monchique study case (Figure 8B) comprises in fact two distinct events that occurred closely in time and space. Starting on the 9th of August in the centre-right area of the burned shape (Figure 8B3), FWI values were not persistently high during this day over this region, reaching about 38 (Figure 8B1) and being close to the mean value (Figure 8B2). Atmospheric instability, however, was high, with values of CHI above 9 (Figure 8B1), nearing one standard deviation above the mean value for this region at this time (Figure 8B2). These high CHI values clearly influenced the FWIe to be greater than those of FWI, therefore, at this time, the atmospheric instability did play a substantial role in increasing the meteorological fire danger FWIe associated with the beginning of this event. As it evolved in the next two days, the FWI increased greatly while the CHI remained essentially unchanged. During these days the greatest FRPs were registered (grey bars in Figure 8B1, do note the logarithmic scale) as most of the burned area in Figure 8B3 is affected. From the 13th of August onwards, a secondary event evolves, eastward of the first one (right side of Figure 8B3) and, at first, FWI values fall substantially with respect to the previous days, while CHI was still large, thus increasing FWIe (Figures 8B1 and 8B2) - a near copy of the situation on August 9th. The following day the FWI increased to the highest values in this study case and, with the aid of the still high CHI, saw the FWIe nearing 60, exceeding the two-standard deviation over the mean value for this region at the time, with a probability of exceedance below 2.5% (Figures 8B1 and 8B2). The last day saw the decrease of the CHI, thus inducing a larger reduction of the FWIe to values identical to those of the FWI, although they were still high; this day coincided with the last FRP observations for this event.

The last study refers to the event which occurred in August 2018, mostly over the area that had already been affected in 2003 as seen in Figure 8A. This case was marked by large fire meteorological danger and with high FRP values being initially captured on the 3rd of August, with FWI values above 50, being two standard deviations above the mean value for this region and presenting a probability of exceedance close to 2.5 % (Figures 8C1 and 8C2). At the beginning, the CHI was high, with values approaching 11, however, the difference was not substantial between FWI and FWIe (Figures 8C1 and 8C2) - a similar behaviour to that of the October 2017 seen in Figure 7. As the days progressed, the FWI decreased while the CHI increased to more exceptional values (near 12), causing the decrease of the FWIe to be slightly less as substantial, and, during these days (more specifically on August 5th) the largest FRPs were registered. The last two days of this event saw the decrease of the atmospheric instability which resulted in the approaching of the FWIe to the FWI values.

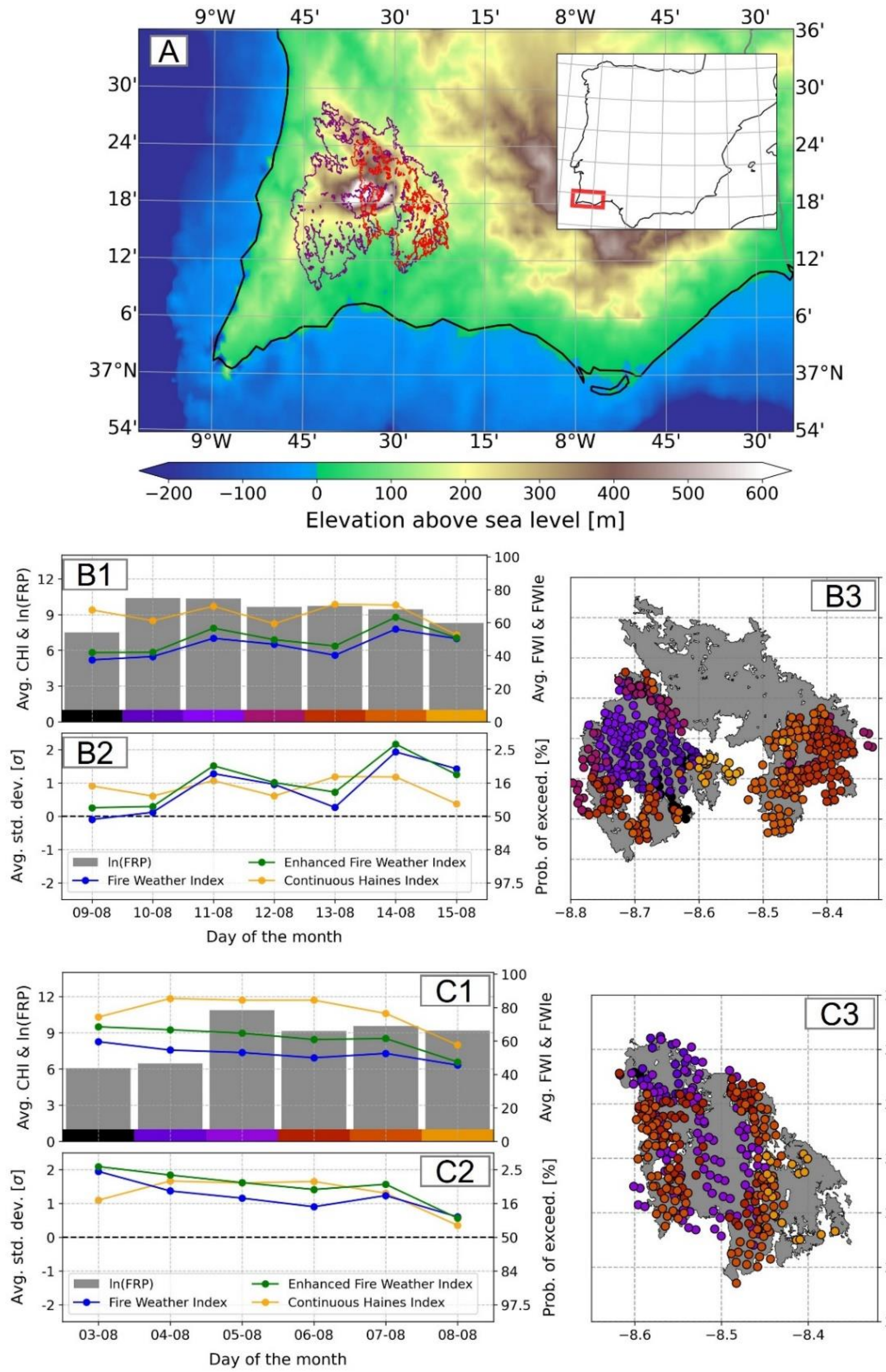

Figure 8 – Study case for the Monchique region. Panel A shows the analysed area, with the shapes representing the burned areas for 2003 (purple) and 2018 (red), topography is shown in colours. Panels B (1-3) and C (1-3) show the respective episodes for 2003 and 2018. Subplots 1 and 2 in these panels are as shown in Figure 6, with the addition of the colours corresponding to the day in subplot 3 that shows the affected region and the FRP location in coloured scatters.

3.5. Discussion on the comparison between reanalysed FWI, FWIe, and CHI

This study comprehensively analysed the relation between atmospheric instability and fire risk, using the novel FWIe, recently developed by Pinto et al. [2020], that associates the well-known instability index coined Continuous Haines index (CHI), and the most widely used meteorological fire danger index, the FWI. This relationship over IP was extensively studied, from a climatological approach for the period 1980 to 2020. Additionally, the observed occurrences of fires with FRP from 2001 to 2020 were compared to several fire danger classes proposed by EFFIS. Finally, several specific case studies were seen to identify the behaviour of the new FWIe in relation to the older FWI and checked the successfulness in assessing better meteorological fire danger over the Iberian region.

A climatological analysis of CHI showed that the largest values of this atmospheric instability metric are located mainly in the southern region of Iberia. This may be attributed to the more complex topography of the region, whereas the northern part of Iberia presents some complex topography, but with substantially lower temperatures, decreasing convective instability. The regions that correspond to the junction of the Baetic Mountains, the Central System, and the Iberian System present the largest values of CHI in summer with an absolute maximum in Sierra Nevada. Regarding FWI and FWIe, the highest values may be found in southern regions, which are not typical fire-prone locations. Indeed, land cover over these areas is mainly cropland and the only vegetated areas are in mountainous regions. The most fire-prone regions are those located in the north-western Iberia, namely the north of Portugal and the Spanish northwest region of Galicia, which, although showing lower values of FWI and FWIe, must be considered as critical regions due to a combination of weather-climate, vegetation, geographical and human factors. Furthermore, the north-western IP is also a crucial region of rising fire danger in the future, especially in the months of June, July, and August. Values of FWIe tend to be on average lower than those of FWI, implying that predominant stable conditions decrease (albeit slightly) the fire risk level given by standard FWI. This may be viewed as an inherent characteristic of the new enhanced FWIe, which favours an increase in the more extreme values to better evaluate the most intense occurrences and down-grades the less dangerous ones.

Besides their seasonal variability, the three indices have significantly increased in the past 4 decades. These increases were prevalent over the warmer months from May to October, especially affecting the meteorological fire danger indices (FWI, FWIe), which had major increases in May, July, and August that belong to the so-called extended fire season. During these warmer months, most of the IP has suffered a significant increase in all three variables, with exception of the north-western part of Iberia in the NW and N clusters for the CHI. Regions SW and E were again found to be the ones characterized by the most significant increments in long-term trends. Maximum decadal trends of FWIe occupied a much larger area compared to FWI, which is expected, since the FWIe incorporates results from the CHI and FWI and those did not have maximum decadal trends coinciding spatially. The specific location of these changes should be further analysed in future studies focused on local scale analysis. Moreover, several studies have predicted an increase in fire danger associated indices, namely the FWI, associated with an increase in mean air temperature in most of the region related to anthropogenic climate change.

Comparing FWI and FWIe, the latter was found useful in differentiating events in which convective meteorological situations help the enhancement of fire risk and eventually fire propagation. This was seen by looking at different classes of observed fire occurrences (in the form of FRP values) and comparing these to the fire danger classes proposed by EFFIS. The comparison between observed FRPs and the calculated FWI and FWIe allowed us to verify that the higher the FRP class (i.e., larger the occurrence) the greater is the probability of the observations falling in the higher FWI classes. In fact, in the two strongest FRP classes (i.e., above 130.1 MW), the biggest FWI classes (i.e., "high" danger up-wards) presented consistently higher FWIe with respect to FWI. These results lead to the conclusion that FWIe better represents the meteorological fire danger in these extreme cases. Overall, our results show that higher FRP classes were more prone to be affected by atmospheric instability than lower meteorological fire danger situations. Moreover, for most of the six FRP classes considered the reverse was also found (with some marginal exceptions), where lower danger classes (i.e., "moderate" danger downwards) presented higher FWI when compared to FWIe. Concluding, it can be stated that higher FRP (i.e., more intense fires) tend to occur in higher FWI values and the FWIe generally increases the meteorological danger in these occurrences while in lower FWI classes, this index remains with greater values compared to the FWIe.

The two case studies of the 2017 Portuguese fire season, that took place on the 17th of June and on the 15th of October, have been thoroughly compared. Results showed that the June episode presented larger convective circulation, which helped propelling the fire intensity, i.e., the CHI was higher, and therefore, the fire risk was much higher. On the other hand, the October episode, had the aggravating passage of Hurricane Ophelia (2017), just west of the Iberian coast, which, despite not directly increasing the convective circulation over the region, increased the wind intensities observed in these areas, which in turn induced increased CHI values. Overall, despite their very different nature and impacts, both extreme fire episodes in 2017 include a high convective potential for fire spreading, although this mechanism was more relevant for the June episodes.

Finally, it was evaluated the role of CHI, FWI and FWIe for the Monchique megafires case studies that occurred in the 2003 and 2018 fire season in southwestern IP. The 2003 covers two August fires, the first that started on the 8th at Marmelete and a second one that initiated on the 12th at Silves. At the beginning of both occurrences, atmospheric instability was found to be substantial in providing an increment to the meteorological fire danger in the form of the FWIe, while at the very end of the episodes the reverse was observed and the value of FWIe fell below of the FWI. In 2018, the event also took place in August, starting on the 3rd near the town of Monchique, 80% of the area affected by this fire had been already burned by the previous fires from 2003. In this case, the FWI presented high values throughout this event although with a small decrease and at the beginning the atmospheric instability was high. As the event progressed the instability increased, attenuating the decrease observed in the FWI during the days with greatest FRPs. At the end of the event both the instability and the meteorological fire danger decreased substantially, helping the end of the event. Both these case studies affected the same general area (the slopes of the Monchique Range) 15 years apart. As previously mentioned, the CHI was observed to be higher in places of topographic complexity and, as these case studies made clear, the atmospheric instability (that is already high in these places) showed exceptional values upwards of 10 (reaching 12, in 2018). Previous studies have pointed out that extreme CHI values above 10 imply that it is extremely complex to extinguish fires and there is an aggravated risk of underpredicted fire behaviour. These facts combined indicate that atmospheric instability played an important role in both events.

3.6. The future of extreme meteorological fire risk under climate change scenarios

FWI distributions from the multi-model ensemble are first compared with those from ERA5 (Figure S6). Results show S scores between modelled and observed PDFs typically above 70%, and S90 scores above 80%, which guarantees that the multi-model ensemble is able not only to reproduce the distribution of observed FWI, but also the tail of the PDF, a critical feature to achieve the objectives of the present work.

Figure 9 shows the ensemble mean monthly average 90th percentile of FWI, FWIe, and the difference between the two, for the historical period (1971 – 2000). These maps help understanding the behaviour of the variables in the extended summer period. As expected, values of fire weather indices increase from June to August and decrease in September. Absolute values of FWI and FWIe vary depending on the latitude, with values of the 90th percentile surpassing 50 in several southern regions in July and August and varying between 5 and 20 in most northern regions. The difference between FWI and FWIe shows a dichotomous behaviour in Iberia. These differences are more evident in July and August, with larger FWIe in the southern halve of the peninsula, and larger FWI mostly located in the northern regions, with particularly large differences in the Ebro region. This is due to variations in CHI (displayed as isolines), which is larger (smaller) in the southern (northern) Peninsula. June and September present somehow similar patterns but with lower differences in the south, with the exception over Ebro in September, where FWI is substantially larger than FWIe.

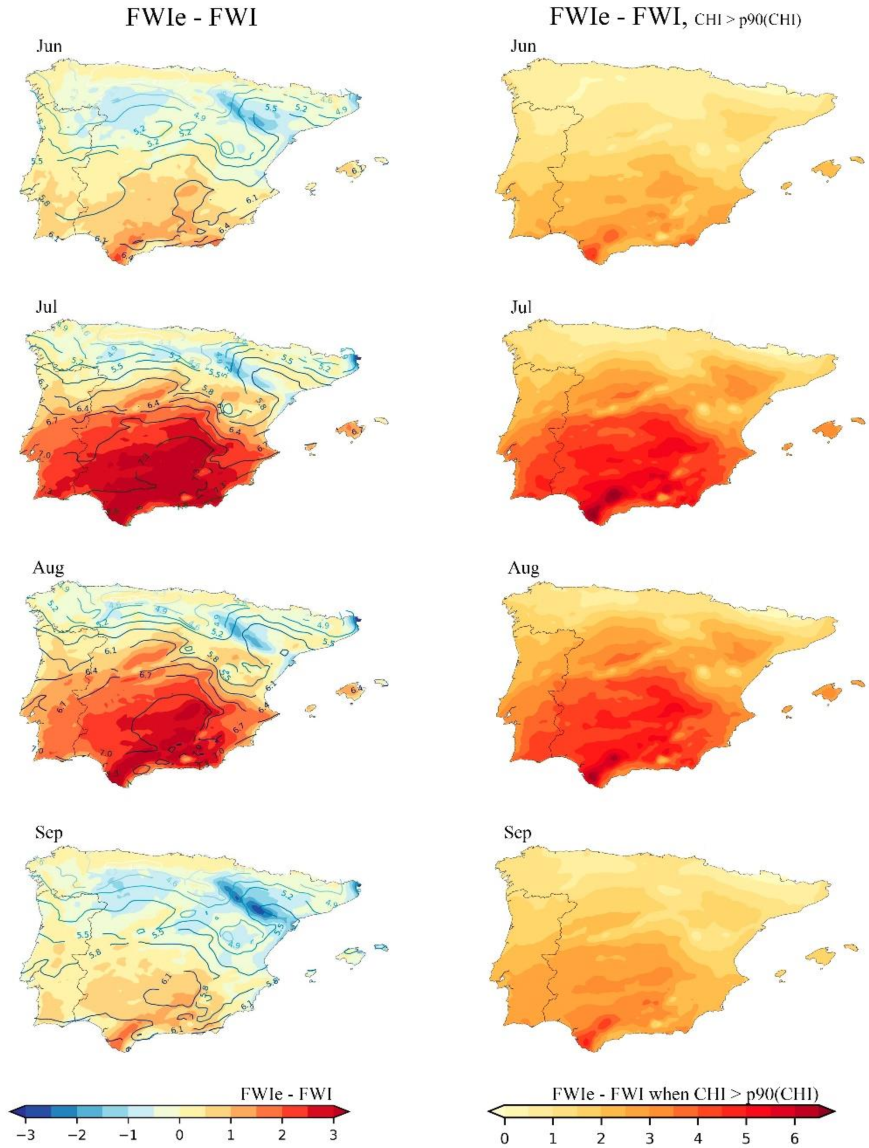

Figure 9 – Ensemble mean of the monthly average 90th percentile for the historical period (1971 – 2000) using a 5-day moving window of FWIe – FWI (left) considering all values of CHI and (right) only considering cases where CHI is larger than its 90th percentile. Contours represent the CHI spatial distribution.

When examining the future projections for FWI, the most substantial increases in the number of extreme FWI days can be found from mid-century onwards for RCP4.5 and RCP8.5 (Figure 10). Here, changes in number of extreme FWI days surpass 100% in many regions, starting in the north-western and central regions for RCP4.5 mid-century (with most of the remaining peninsula surpassing 50% of increase in the number of extreme FWI days). Changes larger than 100% then spread to southern and eastern Iberia in 2071 – 2100 with RCP4.5, and 2041 – 2070 with RCP8.5, and finally occupying all the territory in 2071 – 2100 with RCP8.5. It is worth noticing that the larger increases are observed in the north-western region, with anomalies of more than 45 days, which corresponds to an increase of almost 5 times the historical number of extreme FWI days. Indeed, this implies that the north-western region of Iberia may have a minimum of 57 (45 + 12) days of extreme FWI days in the extended summer JJAS in 2071 – 2100, i.e., near halve of the 4-month summer period considered.

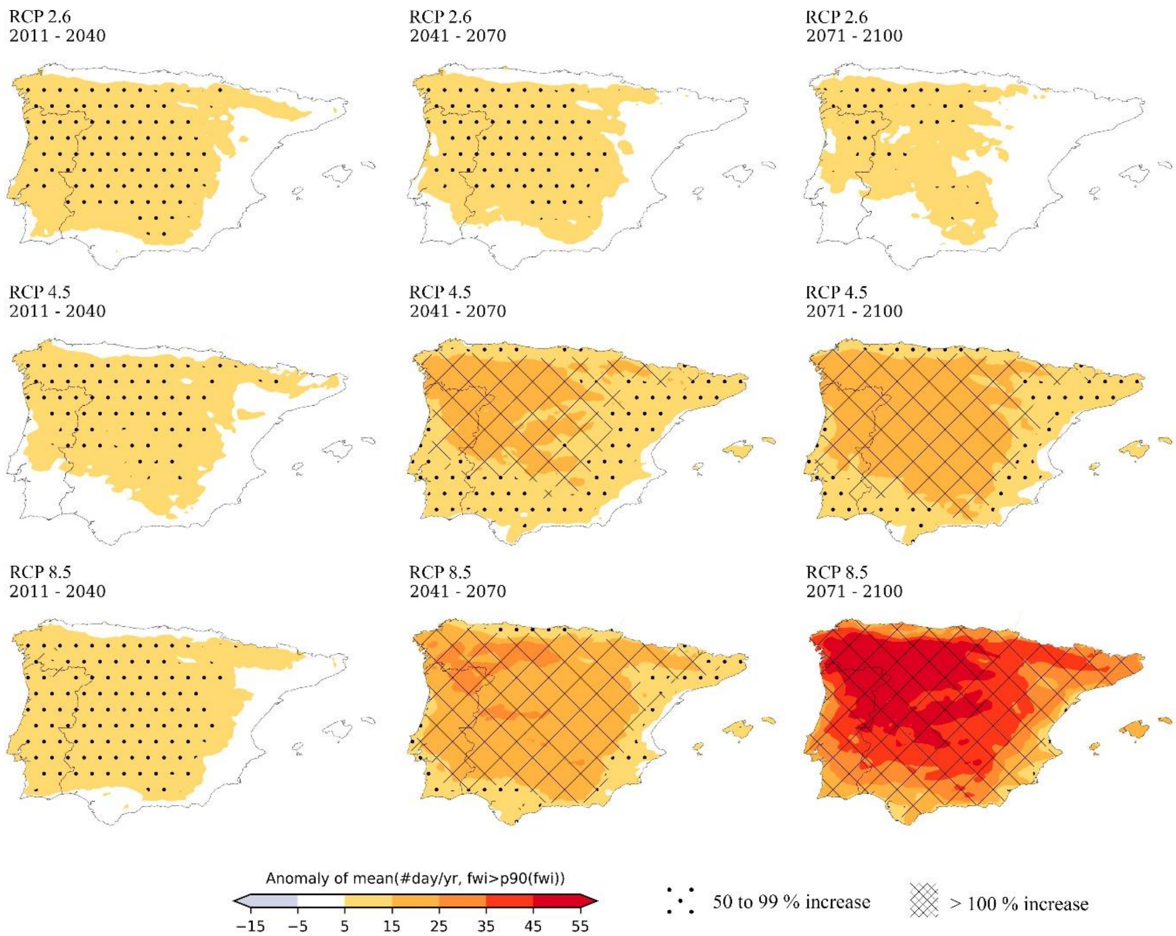

Figure 10 – Anomalous number of days with extreme fire risk measured with FWI per season (JJAS) for (left column) 2011 – 2040, (central column) 2041 – 2070, and (right column) 2071 – 2100 following (top row) RCP 2.6, (middle row) 4.5, and (bottom row) 8.5. Dots indicate an increase between 50 – 99% relative to the historical period and diagonal grid indicates an increase of more than 100% of days with extreme fire risk.

Conversely, northern, eastern, and southern coastal regions for RCP2.6 over all periods, and the 2011 – 2040 over the three RCPs, show virtually non-existent changes (between -5 and 5 days). Nevertheless, for the 2011 – 2040 period and the RCP2.6, results show already several regions where the increase surpasses 50% of historical extreme FWI days (i.e., an increase of at least 6 extreme FWI days). Figure 11 shows equivalent results for FWIe, with a similar behaviour to FWI. However, the increase in the number of days with high fire risk by FWIe is slightly smaller than those given by FWI. The extended summer aggregated results for the anomaly of extreme FWI and FWIe days does not explicit the months where this increase may be pivotal.

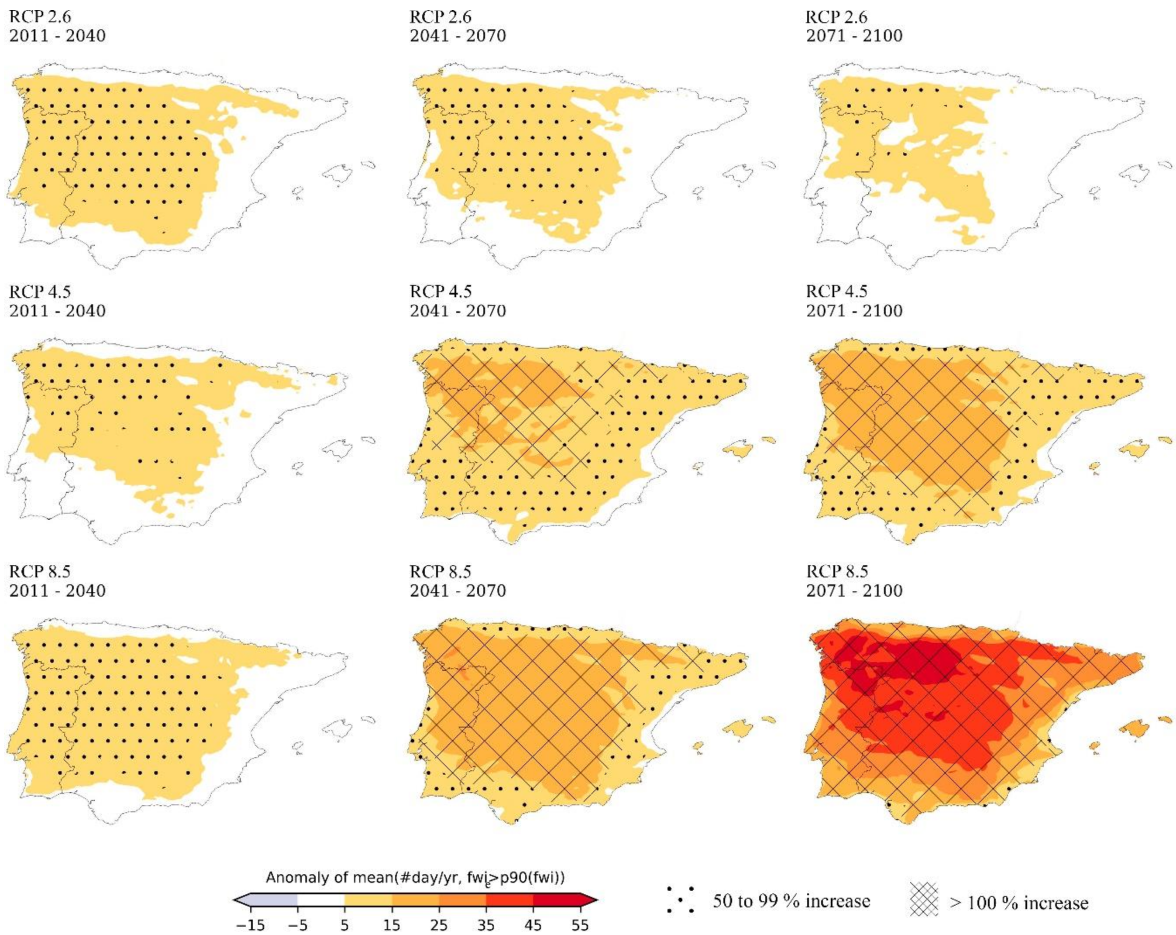

Figure 11 – Anomalous number of days with extreme fire risk measured with FWIe per season (JJAS) for (left column) 2011 – 2040, (central column) 2041 – 2070, and (right column) 2071 – 2100 following (top row) RCP 2.6, (middle row) 4.5, and (bottom row) 8.5. Dots indicate an increase between 50 – 99% relative to the historical period and diagonal grid indicates an increase of more than 100% of days with extreme fire risk.

Hence, Figure 12 shows the anomaly by spatially aggregating in clusters and separating the individual JJAS months. The month with larger anomalies changes according to the four clusters considered. For the NW clusters, the results for RCP4.5 and RCP8.5 show similar anomalies in JJA, with an average of more 5 (4.6) and 11.4 (10.4), respectively, of extreme FWI (FWIe) days per month, at the end of the century. The SW clusters shows a different behaviour with June being the month with larger anomalies of extreme FWI days: 4.6 and 13.0 for RCP4.5 and RCP8.5, respectively, at the end of the century; and FWIe days: 4.2 and 12.1 for RCP4.5 and RCP8.5, respectively, at the end of the century, then progressively decreasing in the subsequent months.

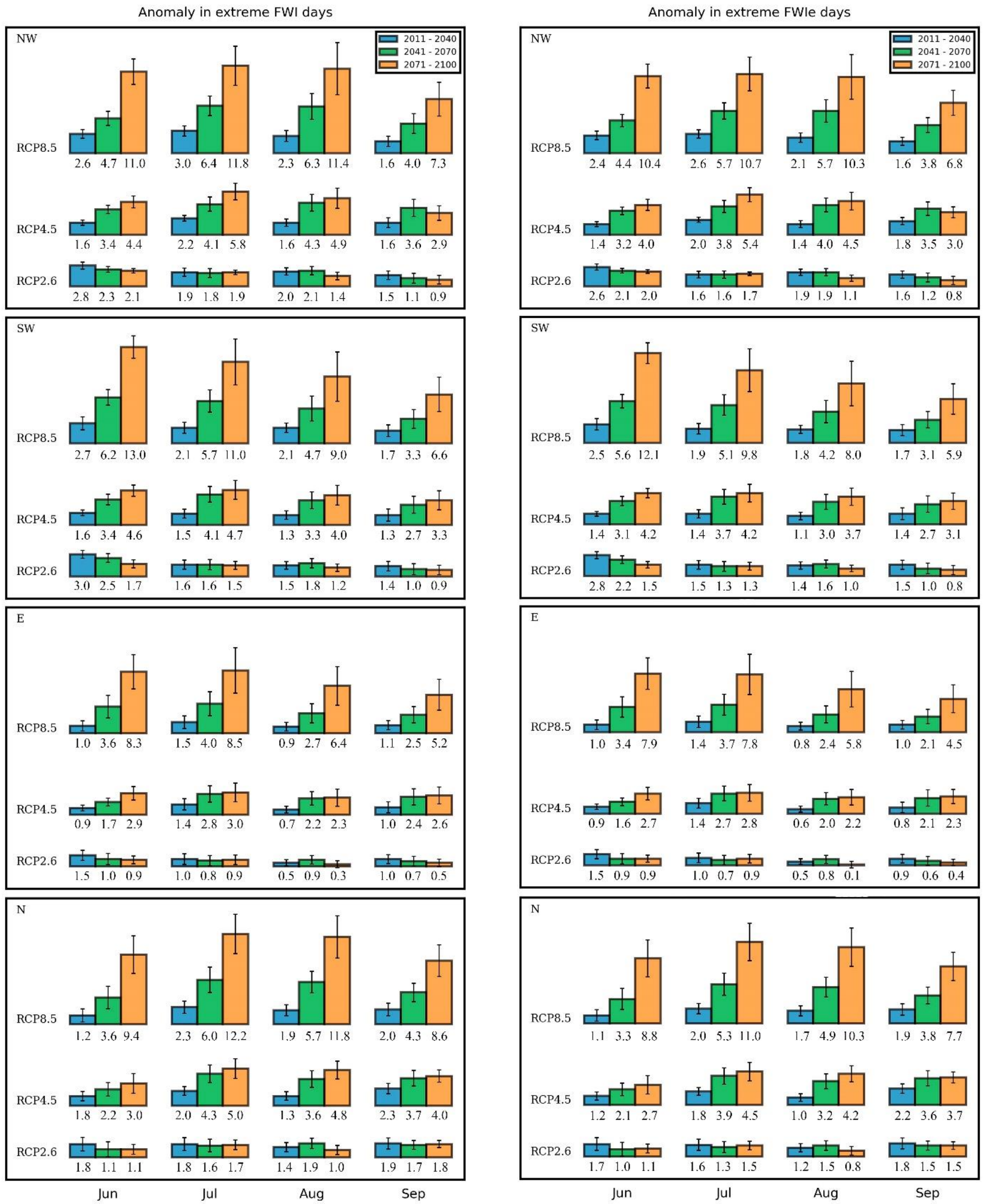

Figure 12 – Spatial mean of the anomalous number of days per month (JJAS) with extreme fire risk for NW, SW, N, and E regions (top to bottom), and for FWI and FWIe (left to right). Bar plots in blue, green, and orange represent 2011 – 2040, 2041 – 2070, and 2071 – 2100, respectively. The value below the bar is the spatial mean of days. The whisker represents the standard deviation.

The E cluster shows a similar behaviour to that of SW, having lower absolute values of anomaly (anomaly of days at end of century vary between 5.2 and 8.5 for RCP8.5 for FWI and 4.5 and 7.9 for RCP8.5 for FWIe). Finally, the N cluster shows alike results as those from NW, with the difference that June shows lower anomalies than July and August. For the 4 clusters, September is consistently the month with lower anomalies, and projections following the RCP2.6 scenario show rather small anomalies without a strong signal distinguishing the months and the different periods.

Figure 13 shows a simple distributional behaviour of the multi-model ensemble of FWI and FWIe for the 4 clusters pre-defined of the Iberian Peninsula, focusing on the evolution of the values over the historical and three future periods of study, and considering the three RCPs. The distributions are shown separately for each individual month of the extended summer as previously defined: June, July, August, and September. As expected, clusters located in the northern (NW, N) peninsula show lower absolute values of FWI and FWIe when compared with southernmost clusters (SW and E clusters). The increase in absolute values of these indices from June to August, and the decrease in September is clearly visible. Results presented in Figure 13 show that values of FWI and FWIe do not considerably change for RCP2.6 over all clusters/months but display a steep increase towards the end-of-century period for both RCP4.5 and RCP8.5. For the latter, differences between historical and end-of-century are larger, as expected. As an example, July shows an increase of the median from ~10 to 20 in NW, ~30 to 40 in SW, ~20 to 30 in E, and ~5 to 12 in N for both FWI and FWIe. Differences between the boxplots of the two fire weather indices are notorious when analysing the medians and extremes. Generally, FWIe presents lower median values than FWI but a larger range between the 10th and 90th percentiles. Differences between FWI and FWIe are better described when looking at empirical cumulative distribution functions (CDFs) as shown in Figure S7a-d for both variables, considering the different periods, RCPs, and months, with bins of 5 units from 0 to 80. Figure 14 displays the differences between the CDFs of FWIe and FWI (FWIe – FWI). Two examples are selected to illustrate this analysis, one with positive CDF differences, and the other with negative differences in the CDF values. These are marked as Ex. 1 and Ex. 2, respectively, in the panel relative to the SW cluster in August for the historical period (panel relative to 2011 – 2040). The selected positive case is situated in the meteorological fire risk class of 15 – 20, where there is a probability of 22 (24) % (not shown) that FWI (FWIe) takes a value belonging to that or lower fire risk classes. The negative case is selected in the 45 – 50 class of fire risk, and here there is a probability of 92 (90) % (not shown) that FWI (FWIe) take a value on that or lower classes. In the former case, the probability of having lower fire risk values is higher for FWIe than FWI. Conversely, the latter case indicates that FWIe is more likely to occur in higher risk classes than FWI.

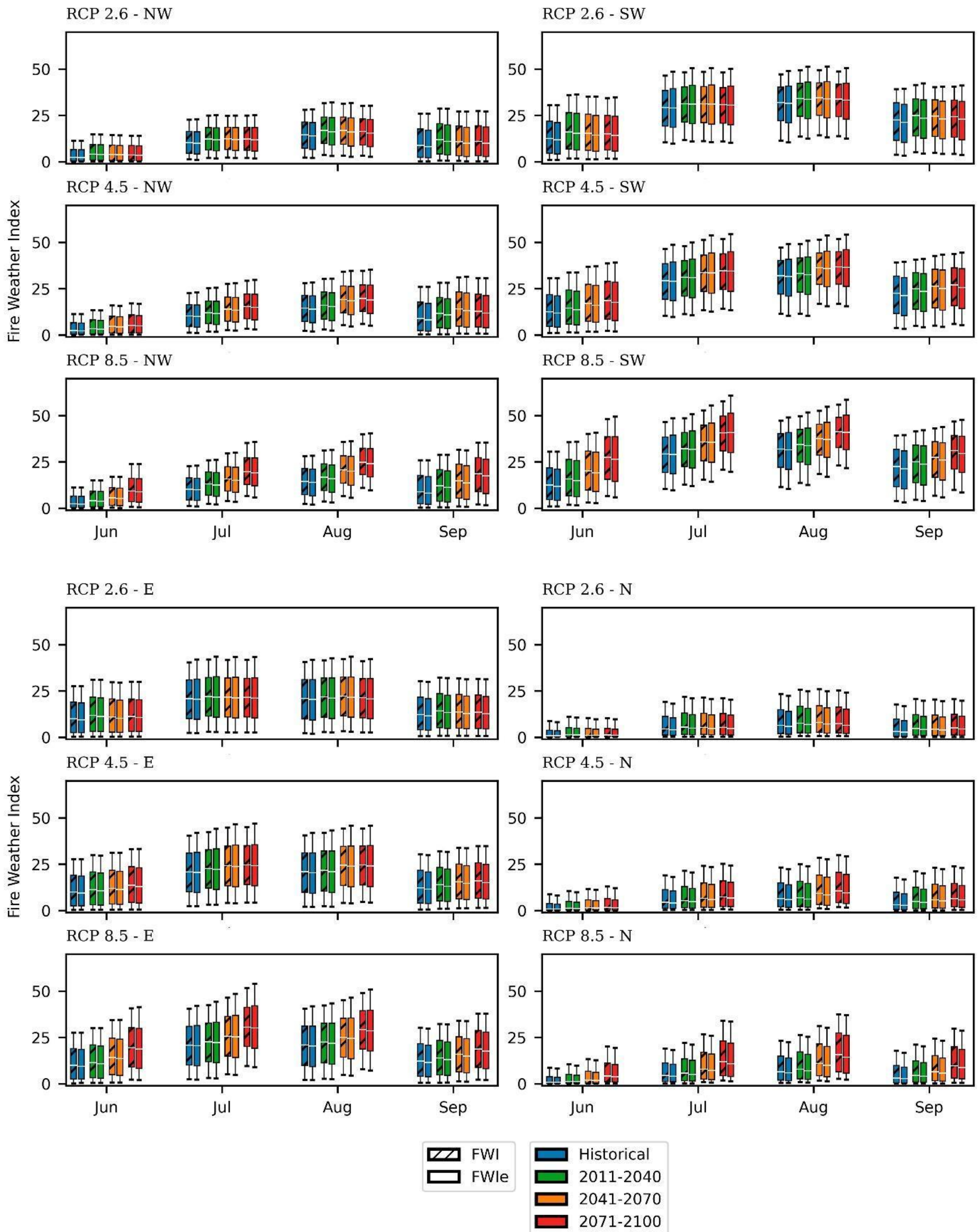

Figure 13 – Monthly (JJAS) comparison of the distribution of FWI (solid with dashes) and FWIe (solid) for historical (blue), 2011 – 2040 (green), 2041 – 2070 (orange), and 2071 – 2100 (red) for the NW (top left), SW (top right), E (bottom left), and N (bottom right). For each region RCP 2.6, RCP 4.5, and RCP 8.5 are shown

(top to bottom). Boxes represent interquartile distance, whiskers represent the 10th and 90th percentiles, and white dash represents the median.

Hence, the general shape of the curves in Figure 14, especially in southern regions and less notoriously in July and August in northern regions, agrees with Figure 13. Indeed, lower and higher extremes of FWIe tend to occur more frequently than FWI, whereas FWI tend to be more frequent for mid-range values. For all clusters it is possible to observe a future shift of the FWI and FWIe CDFs to the right (supplementary material, Figure S7), which is more evident for RCP8.5 at the end of the XXI century. Nevertheless, this shift may also be found at early and mid-century periods. Examples are the month of June in SW for mid-century (supplementary material, Figure S7a), where a substantial shift is already present for RCP4.5 and RCP8.5; or the month of August in NW that shows substantial changes even for RCP2.6 at the beginning of the century (supplementary material, Figure S7). The shift to the right of the corresponding FWIe – FWI curves (Figure 14) is also conspicuous. Once again this is more noticeable for RCP4.5 and RCP8.5, and for the mid- and end- century. This shift implies that the probability of having larger values of fire risk in the future is more likely.

3.7. Discussion on the future extreme fire risk

Intense summer surface heating over land generally favours the development of a thermal low over the central Iberian Peninsula (Hoinka and De Castro 2003). This area is characterized by a semi-arid climate, in which the surface evaporation is reduced, and by the relatively high altitudes of the central Iberian plateau (Gaertner et al 1993). Although the Iberian summer thermal low has shallow convection forms, there is usually no association with the occurrence of precipitation (Trigo et al 2002). The frequent occurrence of a thermal low during the months of July and August may justify the larger values of CHI in Figure 9 and the corresponding larger differences between FWIe and FWI over south-central region of Iberian Peninsula, due to the high instability associated. Nonetheless, the thermal circulation generates strong pressure gradients forcing low-level winds, such as sea breezes, to blow from coast inland, being stronger as the low pressure intensifies (Portela and Castro 1996). In river valleys and mountain passes, an enhancing of these winds occurs as a result of a channelling effect. The strengthening and channelling of the winds from the Mediterranean provides the entrance of warm and humid air into the north-eastern Iberian Peninsula, especially into the Mid Ebro Valley, contributing significantly to the local water balance over the north-eastern mountainous region during summer (Gaertner et al 2001). A significant part of the total annual precipitation over the Ebro basin occurs during autumn, being dominant the stratiform rainfall type, which is less instable than convective type (Martin-Vide and Lopez-Bustins 2006, Iturrioz et al 2007). This is a possible explanation for why FWI is substantially higher than FWIe over the Ebro basin, but more thorough future research on this topic should be pursued.

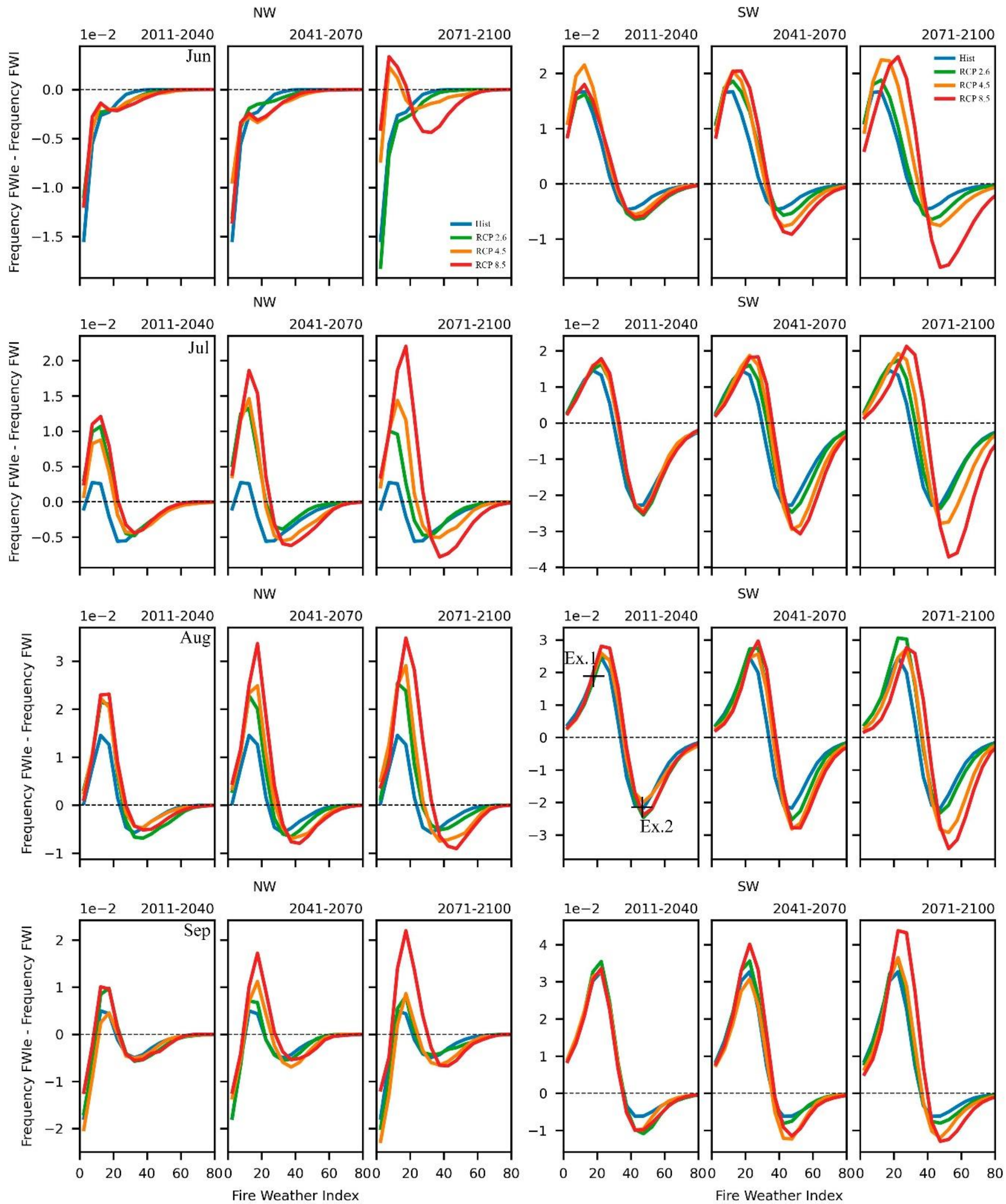

Figure 14 – Differences between CDFs of FWIe and FWI (FWIe – FWI) for NW (left) and SW (right) for the months of JJAS (top to bottom). Ex. 1 and Ex. 2 are examples explained in the text.

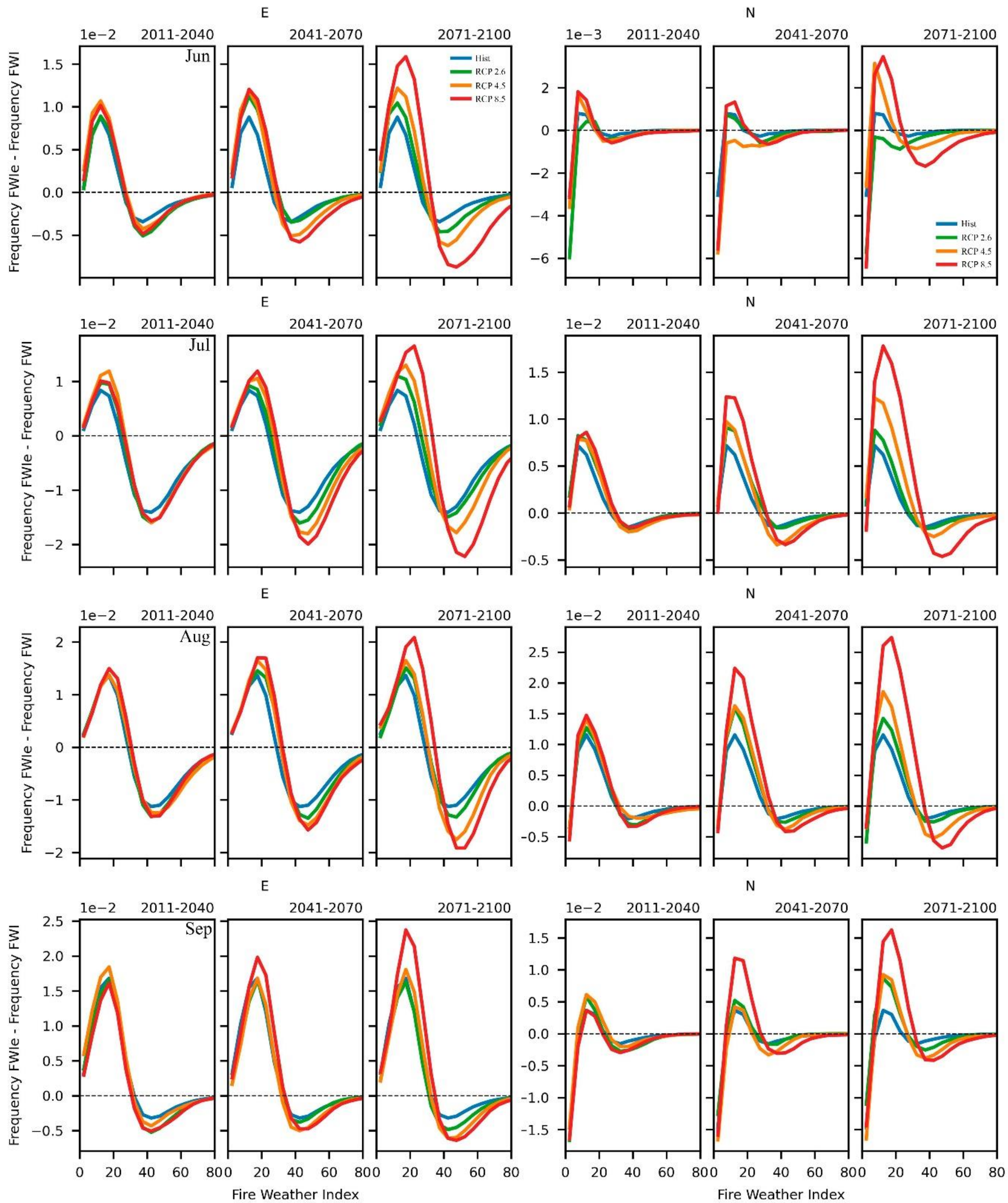

Figure 14 (cont.) – Differences between CDFs of FWIe and FWI (FWIe – FWI) for E (left) and N (right) for the months of JJAS (top to bottom).

The number of summer fire extreme danger days is projected to increase significantly in the future, with the largest anomalies relative to the historical period consistently found in the NW cluster with propensity to extend towards the Iberian central region. These results agree with those obtained in Calheiros et al.

(2021), also based in some of the same CORDEX RCMs, which discussed the future extension of the SW cluster to north. Furthermore, that study pointed to meteorological fire weather risk values increasing considerably when evaluating the historical and future scenarios, especially in late spring and early autumn. However, it is important to note that the authors did not consider fire risk projections driven by the strongly mitigated RCP2.6 scenario. Here, it is showed that besides the increase in extreme danger days in July and August, June also displays relevant increases in most of the clusters. In this case, the SW shows the most striking behaviour of fire danger in June, being even larger than the increases in the traditional fire season months of July and August. This is also in agreement with results by Peña-Ortiz et al (2015), which state that, as a result from the ongoing climate change, summers are becoming longer and with an earlier onset (June). Recent rare destructive events, such as the June 2017 fires in central Portugal (Sánchez-Benítez et al 2018, Turco et al 2019), already support this premise. The disentanglement of variables such as precipitation, minimum and maximum temperature, and wind speed may also be addressed. In that sense, Soares et al. (2017a) showed that for Portugal in summer (JJA) total accumulated precipitation is expected to decrease up to 50% in 2071 – 2100; daily maximum temperature is expected to increase, especially in the northern region, where anomalies may peak at + 6 °C in the late century (Cardoso et al., 2019); daily minimum temperature follows a similar pattern but peaking at anomalies of + 5 °C in the northern region (Cardoso et al., 2019); and daily mean wind speed at 10 m may increase up to + 0.6 m/s (Nogueira et al., 2019), in the RCP8.5.

Results presented in this study show a clear shift to the right of the CDFs of FWIe – FWI, which implies that the probability of having values on the higher classes of fire risk in the future is more likely. This is especially noticeable in scenarios without greenhouse gas emissions mitigation (RCP8.5), but also in some regions with scenarios that include some mitigation (RCP4.5) or strong mitigation (RCP2.6). These results also show that the inclusion of atmospheric instability in the formulation of a fire risk index may be of great importance in the future, especially for monitoring convective wildfires, which are energetic and unpredictable events characterized by the presence of intense atmospheric instability allied with the availability of accumulated fuel (Lareau and Clements 2017). Pinto et al (2020) exemplified the importance of FWIe in convective days such as those occurring during the Monchique (southern Portugal) wildfire of 2018 and Guadalajara (central Spain) wildfire of 2005, with differences between FWI and FWIe reaching 10 in some cases (larger FWIe). The SW and E clusters are those more affected by atmospheric instability and are the ones where FWIe in the future shows larger differences in CDFs to FWI (negative peaks for high FWI classes in Figure 14). This is especially noticeable in July and August in the SW region for RCP8.5 at the end of the century since there is an expected strengthening in the thermal low over central Iberia in the future due to local warming (Cardoso et al 2016, Soares et al 2017c). Conversely, N and NW clusters show larger differences in CDFs between FWIe and FWI for lower fire risk classes (positive peaks for low fire risk classes in Figure 7). This means that there is a tendency to have more values of FWIe in lower classes, i.e., lower values of atmospheric instability in the future, especially in July and August for RCP8.5 in the end of the century. This may be related to future changes in the thermal low characteristics.

Although FWI and FWIe are solely driven by meteorological variables, these results point to a substantial problem of wildfire adaptation and mitigation to climate change in the region. However, it is worth noticing that with a strong mitigation scenario, such as RCP2.6, projections of fire risk are not as drastic as those projected with a no mitigation scenario, such as RCP8.5. However, even meteorological fire risk projections in the context of RCP2.6 show a slight increase of extreme danger days. Hence, adaptation strategies to prevent large ecological, economical, and human losses must be developed by taking several scenarios into account. Of course, the presence of biomass and ignition are critical variables without which a fire cannot occur. Forthcoming work may focus on the relation of vegetation and ignition probabilities, for example by using the new CMIP6 models which have a dynamical vegetation component.

With this study it is presented a comprehensive analysis of future fire risk in the Iberian Peninsula, taking advantage of indices such as FWI, and the state-of-the-art FWIe. The latter was recently shown to be an important asset for fire risk monitoring in the region of study (Pinto et al 2020). Furthermore, the methods used in this study include the use of a state-of-the-art high quality weighted multi-model ensemble developed specifically for the region (Lima et al 2022) and the use of three RCPs from strong to no mitigation and three projected periods (2011 – 2040, 2041 – 2070, and 2071 – 2100). However, is acknowledged that this study presents some caveats. Indeed, a major issue is the impossibility to use variables at noon with EURO-CORDEX RCMs, where variables are usually available at a daily scale. A previous work advocated caution when using daily means instead of instantaneous noon values, arguing that fire danger extremes cannot be reliably transformed from daily to instantaneous to accommodate magnitude and spatial patterns of FWI (Herrera et al 2013). Nevertheless, it must be stressed that the main aim of this work was to look at future projections and to make the first comparison between future projections of FWI and FWIe, including a component of atmospheric instability in Iberia. In this regard the non-use of noon values affects both datasets equally. It is also worth emphasizing that this work deals with meteorological fire danger alone, and therefore, it does not include any variable linked with the occurrence of fires (e.g., Fire Radiative Power). Such endeavour must be tackled in a future assessment linking meteorological fire risk (and its climate change evolution) with ignitions and burned area. Such work should be key to the development of mitigation and adaptation measures in the region. Nevertheless, in terms of designing storylines for adaptation strategies in Portugal and Spain, results from the present study may be considered a relevant regional starting point. Furthermore, it is relevant to stress that in this study RCMs are forced with GCMs from CMIP5, with simulations based on RCPs. In the near future, regional simulations based on CMIP6 will be available with Shared Socioeconomic Pathways (SSPs), which may be an important asset to study the impact of future projections of fire risk in the population.

3.8. Projections of Fire Radiative Power (FRP) and return periods of burnt area

FWI from the historical period presents a strong bias when compared to ERA5. Figure 15 shows the differences between the distributions of FWI from the two databases (top panels, black solid line for ERA5 and purple dashed line for historical multi-model ensemble), concerning both PDFs and CDFs. Historical FWI presents a strong bias to smaller values, where (e.g.) more than 70% of the cases have values lower than 20. On the other hand, FWIs lower than 20 occur in around 52% of the cases for ERA5. After bias correcting historical FWI by an empirical Gumbel quantile mapping method, results show a corrected historical (blue solid line in Figure 15) multi-model ensemble comparable to ERA5 FWIs. Distributions of each pair of GCM-RCM before and after bias correction, in the form of box plots, may be found in the supplementary material. Besides correcting the historical period, the future scenarios are also bias corrected with the same method. Results of the cumulative distributions of multi-model ensemble corrected historical and corrected projected scenarios are shown in Figure 15 (bottom panels). The curve of projected FWIs tends to shift to the right with the passing of the century. For the projected beginning of the century (2011 – 2030[2]), the three scenarios show a slight shift to the right compared to the historical values, with no obvious dominant scenario. Indeed, for a substantial spectrum of the curve, the strong mitigation scenario (RCP 2.6) shows the largest shift to the right (approximately between FWIs of 10 and 25). However, for the rest of the spectrum the curves are almost interchangeable. When looking to the middle of the century and especially to the end of the century, striking differences between scenarios start to be noticeable. For both periods, the RCP 8.5 scenario takes lead with a conspicuous shift to the right when compared with the other RCPs (this is more obvious in the 2071 – 2090 period). As an example, historical FWIs exceed 20 in about 48% of the cases, whereas for the end (middle) of the century the projected exceedance if of ~55% (~55%) for RCP 2.6, ~59% (~59%) for RCP 4.5, and ~67% (~61%) for RCP 8.5. For the upper tale representative of extreme FWI values, historical FWIs exceed 40 in about 4% of the cases, increasing to 6% (9%) for RCP 2.6, 10% (9%) for RCP 4.5, and 15% (12%) for RCP 8.5, for the end (middle) of the century.

[2] Here the period is 20 years instead of the 30 years analysed in the remaining document, because observations of fire radiative power are only available for a period of 20 years, from 2001 to 2020 (from MODIS).

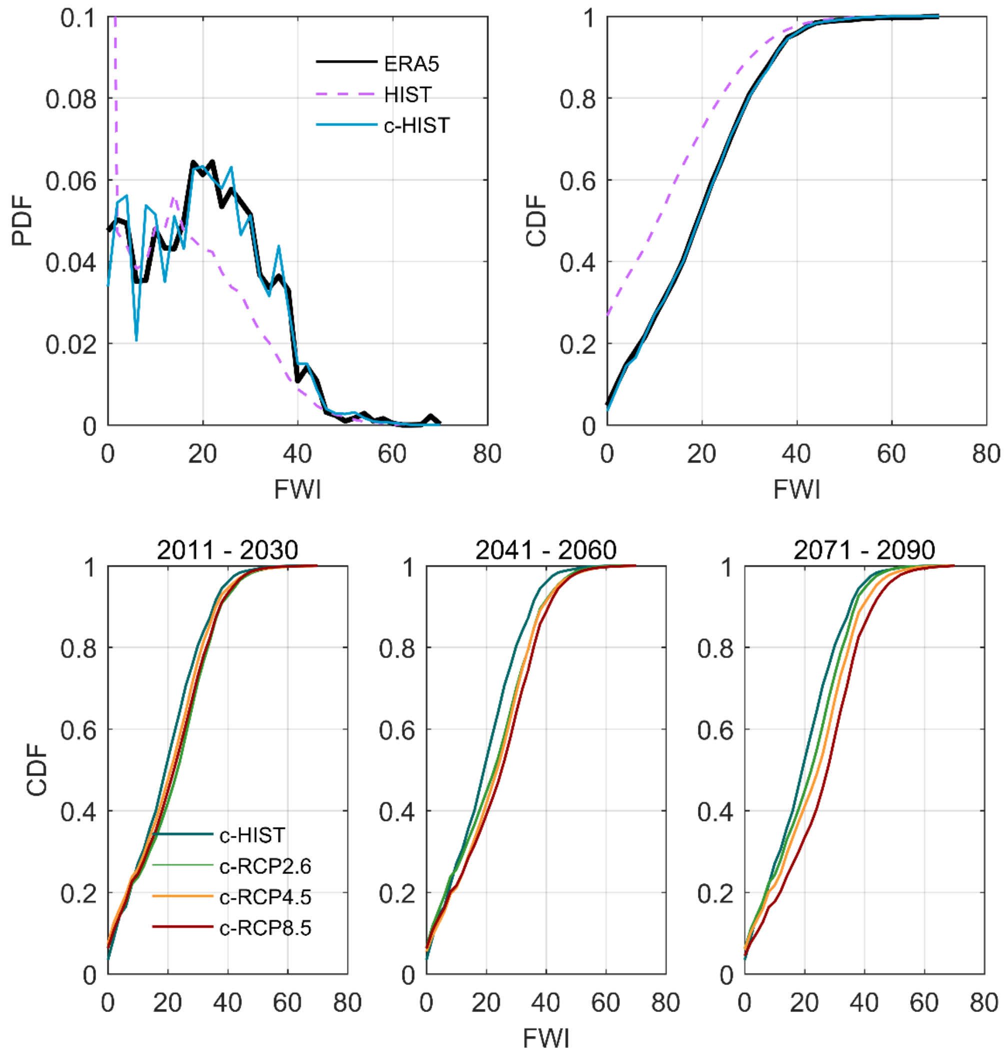

Figure 15 – Distribution of FWI as PDF (top left) and CDF (top right) from ERA5 (solid black line), multi-model ensemble for the historical period (HIST; dashed purple line), and the bias corrected multi-model ensemble for the historical period (c-HIST; solid blue line). CDFs of bias corrected multi-model ensemble FWI for historical and projected scenarios (bottom) RCP 2.6 (green line), RCP 4.5 (orange line), and RCP 8.5 (red line) for the three 20-year periods 2011 – 2030 (left), 2041 – 2060 (middle), and 2071 – 2090 (right).

After synthetically generating values of FRP using the base model with FWI as covariate, a similar procedure to the one presented in Figure 15 is followed to first show the added value of bias correction and then the distribution of historical and projected multi-model ensemble FRP. Figure 16 shows the synthetic FRPs obtained from ERA5 values of FWI (solid black line), non-corrected (dashed purple line) and bias corrected (solid blue line) historical multi-model ensemble. As expected, the non-corrected FRP historical distributions fall apart of those from ERA5 with a substantial bias to lower energies released by fires, and the correction method is able to take the historical distribution to a comparable shape to ERA5 FRPs. The projected scenarios (Figure 16, bottom panels) show cumulative distributions with similar properties to those from FWI. However, it is noticeable that these are closer to each other.

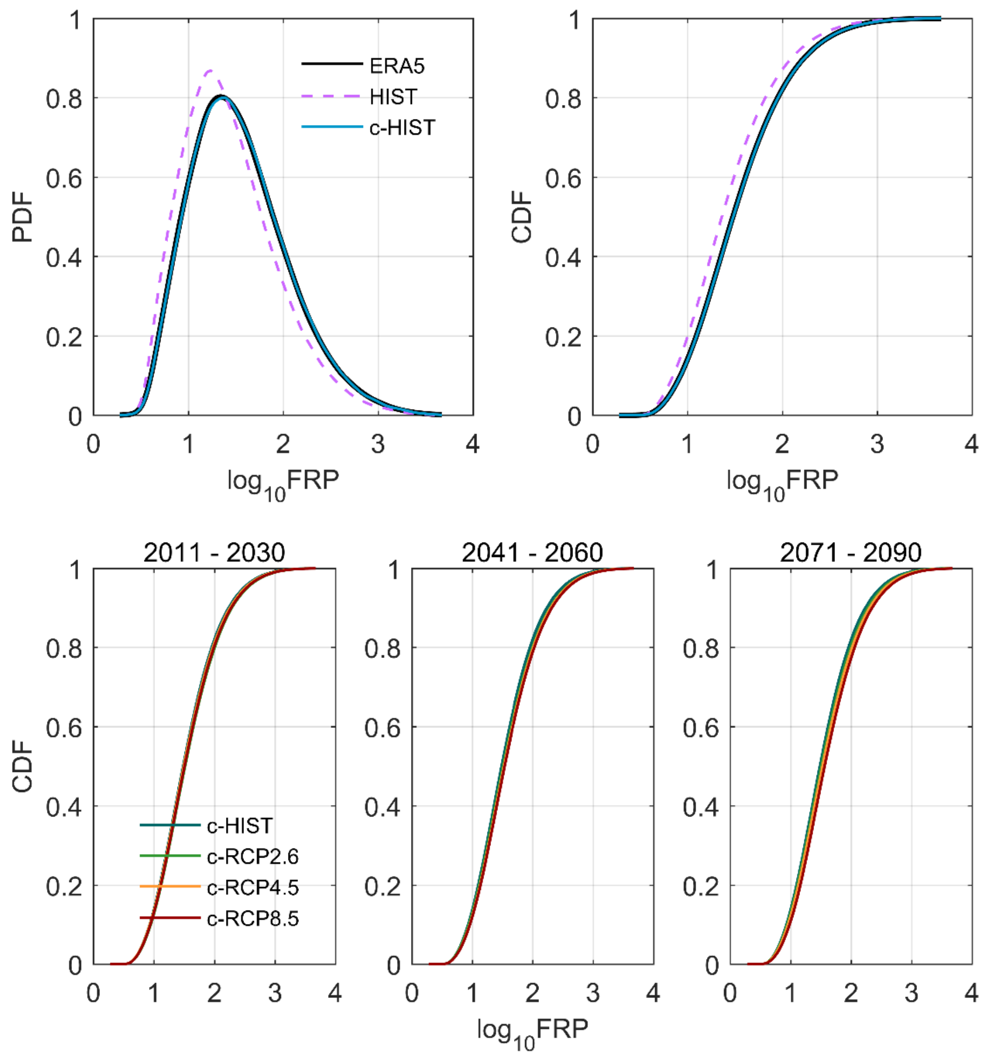

Figure 16 – Distribution of synthetic log10(FRP) as PDF (top left) and CDF (top right) from ERA5 (solid black line), multi-model ensemble for the historical period (HIST; dashed purple line), and the bias corrected multi-model ensemble for the historical period (c-HIST; solid blue line). CDFs of bias corrected multi-model ensemble log10(FRP) for historical and projected scenarios (bottom) RCP 2.6 (green line), RCP 4.5 (orange line), and RCP 8.5 (red line) for the three 20-year periods 2011 – 2030 (left), 2041 – 2060 (middle), and 2071 – 2090 (right).

Hence, to simplify visualization and analysis, the probability of exceedance of a given log10(FRP) in the projected scenarios and periods is divided by the probability of exceedance of that given log10(FRP) in the historical period. This exceedance ratio is shown in Figure 17, where the values of the y-axis represent how many times an event of a given FRP value may occur in the projected scenarios relative to the historical period. Results show a substantial increase in the number of events for larger FRPs. As with FWI, in the beginning of the century the three scenarios are similar between them. However, this means that even for

RCP 2.6 there is a projected increase in events for very intense wildfires: almost 1.5 times the number of events of the historical period for fires with log10(FRP) of 3 (1000 MW), i.e., if four events with intensity larger than 1000 MW occurred in the historical period, these are expected to occur 6 times in the 2011 – 2030 period assuming a strong mitigation scenario. These values tend to increase when the middle and end of the century periods are taken in consideration. For these, and assuming a worst-case scenario (no-mitigation, RCP 8.5), extreme events with log10(FRP) of about 3.5 (about 3000 MW) may occur twofold (middle of the century) or even threefold (end of the century). Nevertheless, when assuming the strong mitigation scenario there seems to be a slight increase of exceedance ratio for extreme events (FRPs between ~1000 – ~3000 MW) in the middle of the century relative to the 2011 – 2030 period, but there is a decrease for the end of the century.

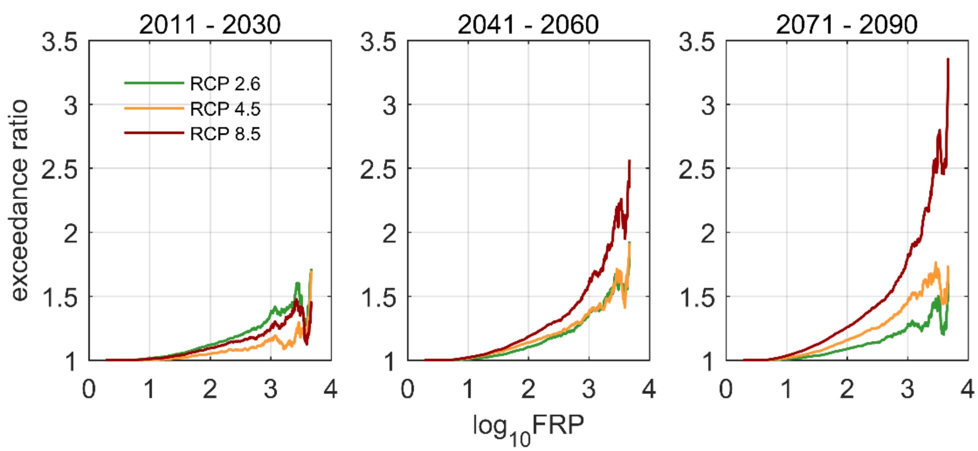

Figure 17 – Exceedance ratio of log10(FRP) projected scenarios RCP 2.6 (green line), RCP 4.5 (orange line), and RCP 8.5 (red line) relative to the historical period for the three 20-year periods 2011 – 2030 (left), 2041 – 2060 (middle), and 2071 – 2090 (right).

In terms of return periods of burnt area in Portugal and NUTS II, the following tables show the results for the ERA5, c-HIST, and projections taking into account the three emission scenarios and the three 30-year future periods. Threshold burn areas chosen to illustrate return periods are 100,000 ha, 150,000 ha, and 200,000 ha. Due to limitations within the model, it is not statistically suitable for the inclusion of larger burnt areas.

Results show that for Portugal, return periods of about 6 to 7 years for burnt areas of 200,000 ha are expected to decrease to about 2 to 3 years for RCP 2.6, about 1.5 to 3 years for RCP 4.5, and about 1 to 2 years for RCP 8.5. The 200,000 ha threshold is especially relevant because since 1995 only three years surpassed this value (2003, 2005, and 2017) (ICNF, 2022). The same procedure was done for the NUTS II regions of Norte and Centro.

Table 2 – Return values (in years) of burnt area for NUTS I for three levels (100,000 ha, 150,000 ha, and 200,000 ha) for ERA5, bias corrected multi-model ensemble for historical and projected scenarios RCP 2.6, RCP 4.5, and RCP 8.5 for the three 30-year periods 2011 – 2040, 2041 – 2070, and 2071 – 2100.

	100,000 ha	**150,000 ha**	**200,000 ha**
ERA5	2.0	3.6	6.9
c-HIST	2.0	3.4	6.5
RCP 2.6 (2011 -2040)	1.3	1.7	2.4
RCP 2.6 (2041 -2070)	1.3	1.8	2.5
RCP 2.6 (2071 -2100)	1.4	1.9	3.0
RCP 4.5 (2011 -2040)	1.4	2.0	2.9
RCP 4.5 (2041 -2070)	1.2	1.4	1.7
RCP 4.5 (2071 -2100)	1.1*	1.3*	1.6*
RCP 8.5 (2011 -2040)	1.2*	1.6*	2.1*
RCP 8.5 (2041 -2070)	1.1*	1.2*	1.5*
RCP 8.5 (2071 -2100)	1.0*	1.1*	1.2*

* Low statistical confidence

Table 3 – Return values (in years) of burnt area for NUTS II (Norte) for three levels (50,000 ha, 75,000 ha, and 150,000 ha) for ERA5, bias corrected multi-model ensemble for historical and projected scenarios RCP 2.6, RCP 4.5, and RCP 8.5 for the three 30-year periods 2011 – 2040, 2041 – 2070, and 2071 – 2100.

	50,000 ha	**75,000 ha**	**150,000 ha**
ERA5	3.3	8.1	20.1
c-HIST	3.1	7.5	20.7
RCP 2.6 (2011 -2040)	1.6	2.7	5.1
RCP 2.6 (2041 -2070)	1.7	2.8	5.3
RCP 2.6 (2071 -2100)	1.8	3.2	6.4
RCP 4.5 (2011 -2040)	1.8	3.1	5.6
RCP 4.5 (2041 -2070)	1.3	1.8	2.6
RCP 4.5 (2071 -2100)	1.3*	1.7*	2.4*
RCP 8.5 (2011 -2040)	1.5*	2.4*	4.0*
RCP 8.5 (2041 -2070)	1.2*	1.5*	1.9*
RCP 8.5 (2071 -2100)	1.1*	1.2*	1.3*

* Low statistical confidence

Table 4 – Return values (in years) of burnt area for NUTS II (Centro) for three levels (50,000 ha, 75,000 ha, and 150,000 ha) for ERA5, bias corrected multi-model ensemble for historical and projected scenarios RCP 2.6, RCP 4.5, and RCP 8.5 for the three 30-year periods 2011 – 2040, 2041 – 2070, and 2071 – 2100.

	75,000 ha	**100,000 ha**	**125,000 ha**
ERA5	3.1	5.3	9.4
c-HIST	3.0	5.1	9.0
RCP 2.6 (2011 -2040)	1.6	2.2	3.0
RCP 2.6 (2041 -2070)	1.8	2.5	3.4
RCP 2.6 (2071 -2100)	1.9	2.9	4.6
RCP 4.5 (2011 -2040)	2.0	2.9	4.2
RCP 4.5 (2041 -2070)	1.4	1.7	2.1
RCP 4.5 (2071 -2100)	1.4*	1.6*	2.1*
RCP 8.5 (2011 -2040)	1.5*	2.0*	2.6*
RCP 8.5 (2041 -2070)	1.2*	1.5*	1.8*
RCP 8.5 (2071 -2100)	1.1*	1.2*	1.3*

* Low statistical confidence

For NUTS II Norte and Centro similar patterns to what is observed in NUTS I are found. Return periods of large burnt areas in both regions show a steep increase in the probability of occurrence. As an example, for Norte, burnt areas of 75,000 ha occurred with a return period of about 8 years in the past and are expected to repeat every 2-3 years in RCP 2.6 and RCP 4.5. For Centro similar results are obtained, with burnt areas of 150,000 ha that occurred with return periods of about 9 years, are projected to occur with periods of 3-4 years in the RCP 2.6 scenario and more frequently in RCP 4.5 and RCP 8.5. The statistical models used here take in consideration the relation between annual observed burnt area in the period 1971 – 2020 and the yearly cumulative Daily Severity Rating (CDSR). It is relevant to note that due to a large shift to the right of the distributions of CDSR within RCP 8.5, the full distribution is without the interval of observations that were calibrated in the model. Hence, there is a low statistical confidence when considering RCP 8.5 scenarios.

4. Final Remarks

This study was performed in the framework of the National Roadmap for Adaptation 2100 – Portuguese Territorial Climate Change Vulnerability Assessment for XXI Century (RNA 2100) project, which is currently being developed with the aim of supporting public policy exercises of adaptation to climate change. This work aims to contribute to the development and assessment of a state-of-the-art of the enhanced fire weather index, the FWIe, which was designed to improve the traditional FWI by incorporating explicitly in its formulation the role played by atmospheric instability. This new enhanced index may represent an important tool, contributing to the forest and wildfire sector decision-makers, since atmospheric instability is known to play a crucial role in the development of some large wildfires. Indeed, this was the case in the deadly wildfires that occurred in Portugal in June 2017, as shown by the case-study analysed in this study. Additionally, from a more structural perspective, this work aims at assessing FWIe by using ERA5 reanalysed data and paves the way to the development of storylines focused on destructive wildfire events in a climate change context, contributing to the development of timely adaptation strategies. This work overall highlights the significant importance of atmospheric instability in the development of extreme fire risk events, providing essential evidence to improve early warning systems in place to prevent large catastrophes from happening, such as the increased effectiveness of the FWIe to predict more or less extreme danger situations comparatively to the more established FWI. Future developments in the area are therefore recommended both locally, regarding potential links with land cover and geographical features such as river basins, near-shore locations, or mountainous areas, or on a more policy level with better territorial planning and vegetation management. Directed to vulnerable forest territories with high fire risk, National Landscape Transformation Programme (PTP) aims to promote a landscape transformation towards a resilient, sustainable, and added value territory. The implementation of PTP in the medium and long term is carried out through four programmatic measures: Landscape Planning and Management Programmes (PRGP), Integrated Areas for Landscape Management (AIGP) and Integrated Operations for Landscape Management (OIGP), Condominium Villages and Parcelling for land use planning.

Here, it is presented a continuation of previous works related with the assessment and characterization of climate change impacts on a number of main climate variables and extremes from highly- to non-mitigated emission scenarios based on a multi-variable constrained ensemble. In the scope of this project, climate change projections of FWI and the new state-of-the-art FWIe were compared. A multi-model ensemble with 13 RCMs was used for historical (1971 – 2000) and three future periods (2011 – 2040, 2041 – 2070, 2071 – 2100) in agreement with RCP 2.6, RCP 4.5, and RCP 8.5. Results indicate that summer days with extreme FWI and FWIe are expected to substantially increase in the future for scenarios RCP 4.5 and RCP 8.5, with an extension of the danger period to June and, in lower magnitude, to September. The north-western region of Iberia, encapsulating the north of Portugal and the north-western-to-central Spain, are the regions with larger increases in meteorological fire danger. This may lead to especially dramatic consequences since these regions are vastly forested. Nevertheless, projections point to little future fire risk increases in the context of RCP 2.6, which in comparison with RCP 4.5 and RCP 8.5 will require less adaptation needs. A sensitivity analysis to forest management and their vulnerability to wildfires is an important step that needs to take place next. Future work exploring the relationship between meteorological indices such as FWI and FWIe and type of vegetation is crucial. However, the issue of vegetation projections and how to include them in the RCMs needs further analysis. The new CMIP6 projections, with dynamic vegetation, may be an important asset for such studies. On this context, work is being done within the Landscape Planning and Management Programmes (PRGP). These programmes design the most adequate landscape and define a medium to long-term transition land-use matrix, supported by a financing model that ensures the transformation of the most vulnerable territory. This matrix transition aims risk prevention and adaptation to climate change, through landscape planning and management and the adoption of specific intervention measures. The execution of the PRGPs is carried out through AIGP and OIGP: the AIGP objective is to promote the management and development of agroforestry spaces in areas of small property and high fire risk; the OIGP will define, in space and time, the intervention programming, the operating model, the financial resources to be allocated and the management and monitoring system.

Incorporated in the RNA 2100 project, the work presented on this report, aims at being a baseline to timely prepare forest wildfire adaptation measures, and to further translate into storylines articulated and integrated with the stakeholders' and policymakers' point-of-view.

Mitigation and adaptation to climate change is a key subject to society, which significance is noticeably growing in the last years with increasing media coverage, social rallies, and political discourse. This is exponentiated when "once in a lifetime" extreme events become more frequent, and authorities struggle to adequately respond due to their magnitude and due to operational impracticality. Indeed, high energy release wildfires with enough fuel to burn for kilometres non-stop are virtually impossible to dominate by the authorities regardless of preparedness and resources. Some examples are the 2020 record breaking fire season on California, the 2020 megafire in Australia, or the 2017 fire season in Portugal. Here it was showed that, for mainland Portugal, very energetic fires (with more than 1000 MW of energy released) may occur 1.5 to more than three-fold depending on the mitigation pathway that is followed, with the nuance that even if the high mitigation scenario is achieved the probability of having megafires is increased by around 1.5-fold. Such result points to the need to adapt regardless of the mitigation scenario followed. Ad-hoc strategies may work for small to medium fires, but for very large fires concrete strategies must be timely prepared and employed either politically and socially, with a new mindset paradigm focused on caution and preservation. Indeed, results presented in this study show that if 95% of the expected fires do not happen in the most extreme fire risk days (>95th percentile of FWI), then the reduction of wildfires with energy above 1000 MW is between 20 and 60%. This is a promising result that shows that there is no need for more restrictive, expensive, and authority focused policies during the months of summer.

5. References

Alessandri A, de Felice M, Zeng N, et al (2014) Robust assessment of the expansion and retreat of Mediterranean climate in the 21st century. Sci Rep 4:1–8. https://doi.org/10.1038/srep07211

Augusto S, Ratola N, Tarín-Carrasco P, et al (2020) Population exposure to particulate-matter and related mortality due to the Portuguese wildfires in October 2017 driven by storm Ophelia. Environ Int 144:106056. https://doi.org/10.1016/j.envint.2020.106056

Bento VA, Russo A, Gouveia CM, Dacamara CC (2022) Recent change of burned area associated with summer heat extremes over Iberia. Int J Wildland Fire 31:658–669. https://doi.org/10.1071/WF21155

Boberg F, Berg P, Thejll P, et al (2009) Improved confidence in climate change projections of precipitation evaluated using daily statistics from the PRUDENCE ensemble. Clim Dyn 32:1097–1106. https://doi.org/10.1007/s00382-008-0446-y

Boer MM, Resco de Dios V, Bradstock RA (2020) Unprecedented burn area of Australian mega forest fires. Nat Clim Chang 10:171–172. https://doi.org/10.1038/s41558-020-0716-1

Brunner L, Lorenz R, Zumwald M, Knutti R (2019) Quantifying uncertainty in European climate projections using combined performance-independence weighting. Environmental Research Letters 14:124010. https://doi.org/10.1088/1748-9326/ab492f

Calheiros T, Pereira MG, Nunes JP (2021) Assessing impacts of future climate change on extreme fire weather and pyro-regions in Iberian Peninsula. Science of The Total Environment 754:142233. https://doi.org/10.1016/J.SCITOTENV.2020.142233

Cardoso RM, Soares PMM (2022) Is there added value in the EURO-CORDEX hindcast temperature simulations? Assessing the added value using climate distributions in Europe. International Journal of Climatology. https://doi.org/10.1002/joc.7472

Cardoso RM, Soares PMM, Lima DCA, Miranda PMA (2019a) Mean and extreme temperatures in a warming climate: EURO CORDEX and WRF regional climate high-resolution projections for Portugal. Clim Dyn 52:129–157. https://doi.org/10.1007/s00382-018-4124-4

Cardoso RM, Soares PMM, Lima DCA, Miranda PMA (2019b) Mean and extreme temperatures in a warming climate: EURO CORDEX and WRF regional climate high-resolution projections for Portugal. Clim Dyn 52:129–157. https://doi.org/10.1007/s00382-018-4124-4

Cardoso RM, Soares PMM, Lima DCA, Semedo A (2016) The impact of climate change on the Iberian low-level wind jet: EURO-CORDEX regional climate simulation. Tellus, Series A: Dynamic Meteorology and Oceanography 68:29005. https://doi.org/10.3402/tellusa.v68.29005

Careto JAM, Soares PMM, Cardoso RM, et al (2022a) Added value of EURO-CORDEX high-resolution downscaling over the Iberian Peninsula revisited – Part 1: Precipitation. Geosci Model Dev 15:2635–2652. https://doi.org/10.5194/gmd-15-2635-2022

Careto JAM, Soares PMM, Cardoso RM, et al (2022b) Added value of EURO-CORDEX high-resolution downscaling over the Iberian Peninsula revisited – Part 2: Max and min temperature. Geosci Model Dev 15:2653–2671. https://doi.org/10.5194/gmd-15-2653-2022

Carvalho A, Flannigan MD, Logan KA, et al (2009) The impact of spatial resolution on area burned and fire occurrence projections in Portugal under climate change. Clim Change 98:177–197. https://doi.org/10.1007/s10584-009-9667-2

Christensen JH, Kjellström E, Giorgi F, et al (2010) Weight assignment in regional climate models. Clim Res 44:179–194. https://doi.org/10.3354/cr00916

DaCamara CC, Calado TJ, Ermida SL, et al (2014) Calibration of the Fire Weather Index over Mediterranean Europe based on fire activity retrieved from MSG satellite imagery. Int J Wildland Fire 23:945–958. https://doi.org/10.1071/WF13157

Diffenbaugh NS, Giorgi F (2012) Climate change hotspots in the CMIP5 global climate model ensemble. Clim Change 114:813–822. https://doi.org/10.1007/s10584-012-0570-x

Eyring V, Cox PM, Flato GM, et al (2019) Taking climate model evaluation to the next level. Nat Clim Chang 9:102–110. https://doi.org/10.1038/s41558-018-0355-y

Faggian P (2018) Estimating fire danger over Italy in the next decades. EuroMediterr J Environ Integr 3:1–13. https://doi.org/10.1007/s41207-018-0053-1

Fargeon H, Pimont F, Martin-StPaul N, et al (2020) Projections of fire danger under climate change over France: where do the greatest uncertainties lie? Clim Change 160:479–493. https://doi.org/10.1007/s10584-019-02629-w

Gaertner MA, Christensen OB, Prego JA, et al (2001) The impact of deforestation on the hydrological cycle in the western Mediterranean: an ensemble study with two regional climate models. Clim Dyn 17:857–873. https://doi.org/10.1007/s003820100151

Gaertner MA, Fernandez C, Castro M (1993) A two-dimensional simulation of the Iberian summer thermal low. Mon Weather Rev 121:2740–2756. https://doi.org/10.1175/1520-0493(1993)121<2740:ATDSOT>2.0.CO;2

García-Herrera R, Garrido-Perez JM, Barriopedro D, et al (2019) The European 2016/17 drought. J Clim 32:3169–3187. https://doi.org/10.1175/JCLI-D-18-0331.1

Giannakopoulos C, le Sager P, Bindi M, et al (2009) Climatic changes and associated impacts in the Mediterranean resulting from a 2 °C global warming. Glob Planet Change 68:209–224. https://doi.org/10.1016/j.gloplacha.2009.06.001

Giorgi F, Jones C, Asrar G (2009) Addressing climate information needs at the regional level: the CORDEX framework. WMO Bulletin

Goss M, Swain DL, Abatzoglou JT, et al (2020) Climate change is increasing the likelihood of extreme autumn wildfire conditions across California. Environmental Research Letters 15:094016. https://doi.org/10.1088/1748-9326/ab83a7

Gouveia CM, Bistinas I, Liberato MLR, et al (2016) The outstanding synergy between drought, heatwaves and fuel on the 2007 Southern Greece exceptional fire season. Agric For Meteorol 218–219:135–145. https://doi.org/10.1016/j.agrformet.2015.11.023

Haines DA (1988) A lower atmospheric severity index for wildland fires. National Weather Digest 13:23–27

Herrera S, Bedia J, Gutiérrez JM, et al (2013) On the projection of future fire danger conditions with various instantaneous/mean-daily data sources. Clim Change 118:827–840. https://doi.org/10.1007/s10584-012-0667-2

Herrera S, Soares PMM, Cardoso RM, Gutiérrez JM (2020) Evaluation of the EURO-CORDEX Regional Climate Models Over the Iberian Peninsula: Observational Uncertainty Analysis. Journal of Geophysical Research: Atmospheres 125. https://doi.org/10.1029/2020JD032880

Hersbach H, Bell B, Berrisford P, et al (2019) Global reanalysis: goodbye ERA-Interim, hello ERA5. ECMWF Newsletter 159:17–24

Hoinka KP, de Castro M (2003) The Iberian Peninsula thermal low. Quarterly Journal of the Royal Meteorological Society 129:1491–1511. https://doi.org/10.1256/qj.01.189

Iturrioz I, Hernández E, Ribera P, Queralt S (2007) Instability and its relation to precipitation over the Eastern Iberian Peninsula. Advances in Geosciences 10:45–50. https://doi.org/10.5194/adgeo-10-45-2007

Jacob D, Petersen J, Eggert B, et al (2014) EURO-CORDEX: New high-resolution climate change projections for European impact research. Reg Environ Change 14:563–578. https://doi.org/10.1007/s10113-013-0499-2

Jacob D, Teichmann C, Sobolowski S, et al (2020) Regional climate downscaling over Europe: perspectives from the EURO-CORDEX community. Reg Environ Change 20:1–20. https://doi.org/10.1007/s10113-020-01606-9

Katragkou E, Garciá-Diéz M, Vautard R, et al (2015) Regional climate hindcast simulations within EURO-CORDEX: Evaluation of a WRF multi-physics ensemble. Geosci Model Dev 8:603–618. https://doi.org/10.5194/gmd-8-603-2015

Keeley JE, Syphard AD (2021) Large California wildfires: 2020 fires in historical context. Fire Ecology 17:1–11. https://doi.org/10.1186/s42408-021-00110-7

Knutti R, Sedláček J, Sanderson BM, et al (2017) A climate model projection weighting scheme accounting for performance and interdependence. Geophys Res Lett 44:1909–1918. https://doi.org/10.1002/2016GL072012

Kotlarski S, Keuler K, Christensen OB, et al (2014) Regional climate modeling on European scales: a joint standard evaluation of the EURO-CORDEX RCM ensemble. Geosci Model Dev 7:1297–1333. https://doi.org/10.5194/gmd-7-1297-2014

Lareau NP, Clements CB (2017) The mean and turbulent properties of a wildfire convective plume. J Appl Meteorol Climatol 56:2289–2299. https://doi.org/10.1175/JAMC-D-16-0384.1

Libonati R, Pereira JMC, da Camara CC, et al (2021) Twenty-first century droughts have not increasingly exacerbated fire season severity in the Brazilian Amazon. Sci Rep 11:1–13. https://doi.org/10.1038/s41598-021-82158-8

Lima DCA, Lemos G, Bento VA, et al (2023) A multi-variable constrained ensemble of regional climate projections under multi-scenarios for Portugal – Part I: An overview of impacts on means and extremes. Clim Serv 30:100351. https://doi.org/10.1016/j.cliser.2023.100351

Lorenz R, Herger N, Sedláček J, et al (2018) Prospects and Caveats of Weighting Climate Models for Summer Maximum Temperature Projections Over North America. Journal of Geophysical Research: Atmospheres 123:4509–4526. https://doi.org/10.1029/2017JD027992

Martin-Vide J, Lopez-Bustins JA (2006) The Western Mediterranean Oscillation and rainfall in the Iberian Peninsula. International Journal of Climatology 26:1455–1475. https://doi.org/10.1002/joc.1388

Mills GA, McCaw L (2010) Atmospheric Stability Environments and Fire Weather in Australia - extending the Haines Index

Moemken J, Reyers M, Feldmann H, Pinto JG (2018) Future Changes of Wind Speed and Wind Energy Potentials in EURO-CORDEX Ensemble Simulations. Journal of Geophysical Research: Atmospheres 123:6373–6389. https://doi.org/10.1029/2018JD028473

Molina-Terrén DM, Xanthopoulos G, Diakakis M, et al (2019) Analysis of forest fire fatalities in Southern Europe: Spain, Portugal, Greece and Sardinia (Italy). Int J Wildland Fire 28:85–98. https://doi.org/10.1071/WF18004

Moriondo M, Good P, Durao R, et al (2006) Potential impact of climate change on fire risk in the Mediterranean area. Clim Res 31:85–95. https://doi.org/10.3354/cr031085

Moss RH, Edmonds JA, Hibbard KA, et al (2010) The next generation of scenarios for climate change research and assessment. Nature 463:747–756

Nogueira M, Soares PMM, Tomé R, Cardoso RM (2019) High-resolution multi-model projections of onshore wind resources over Portugal under a changing climate. Theor Appl Climatol 136:347–362. https://doi.org/10.1007/s00704-018-2495-4

Oliveira M, Delerue-Matos C, Pereira MC, Morais S (2020) Environmental particulate matter levels during 2017 large forest fires and megafires in the center region of Portugal: A public health concern? Int J Environ Res Public Health 17. https://doi.org/10.3390/ijerph17031032

Parente J, Pereira MG, Amraoui M, Fischer EM (2018) Heat waves in Portugal: Current regime, changes in future climate and impacts on extreme wildfires. Science of the Total Environment 631–632:534–549. https://doi.org/10.1016/j.scitotenv.2018.03.044

Pausas JG, Fernández-Muñoz S (2012) Fire regime changes in the Western Mediterranean Basin: From fuel-limited to drought-driven fire regime. Clim Change 110:215–226. https://doi.org/10.1007/s10584-011-0060-6

Peña-Ortiz C, Barriopedro D, García-Herrera R (2015) Multidecadal variability of the summer length in Europe. J Clim 28:5375–5388. https://doi.org/10.1175/JCLI-D-14-00429.1

Pereira MG, Trigo RM, da Camara CC, et al (2005) Synoptic patterns associated with large summer forest fires in Portugal. Agric For Meteorol 129:11–25. https://doi.org/10.1016/j.agrformet.2004.12.007

Perkins SE, Pitman AJ, Holbrook NJ, McAneney J (2007) Evaluation of the AR4 climate models' simulated daily maximum temperature, minimum temperature, and precipitation over Australia using probability density functions. J Clim 20:4356–4376. https://doi.org/10.1175/JCLI4253.1

Pinto MM, Dacamara CC, Hurduc A, et al (2020) Enhancing the fire weather index with atmospheric instability information. Environmental Research Letters 15:940–947. https://doi.org/10.1088/1748-9326/ab9e22

Pinto MM, et. al. (2018) The extreme weather conditions behind the destructive fires of June and October 2017 in Portugal. In: Advances in forest fire research 2018. Imprensa da Universidade de Coimbra, pp 138–145

Portela A, Castro M (1996) Summer thermal lows in the Iberian peninsula: A three-dimensional simulation. Quarterly Journal of the Royal Meteorological Society 122:1–22. https://doi.org/10.1002/qj.49712252902

Prein AF, Gobiet A, Truhetz H, et al (2016) Precipitation in the EURO-CORDEX 0.11∘ and 0.44∘ simulations: high resolution, high benefits? Clim Dyn 46:383–412. https://doi.org/10.1007/s00382-015-2589-y

Ramos AM, Russo A, DaCamara CC, et al (2023) The compound event that triggered the destructive fires of October 2017 in Portugal. iScience 106141. https://doi.org/10.1016/J.ISCI.2023.106141

Riahi K, Rao S, Krey V, et al (2011) RCP 8.5-A scenario of comparatively high greenhouse gas emissions. Clim Change 109:33–57. https://doi.org/10.1007/s10584-011-0149-y

Rodrigues M, Jiménez-Ruano A, de la Riva J (2019) Fire regime dynamics in mainland Spain. Part 1: Drivers of change. Science of the Total Environment 721:135841. https://doi.org/10.1016/j.scitotenv.2019.135841

Ruffault J, Curt T, Martin-Stpaul NK, et al (2018) Extreme wildfire events are linked to global-change-type droughts in the northern Mediterranean. Natural Hazards and Earth System Sciences 18:847–856. https://doi.org/10.5194/nhess-18-847-2018

Ruffault J, Curt T, Moron V, et al (2020) Increased likelihood of heat-induced large wildfires in the Mediterranean Basin. Sci Rep 10:1–9. https://doi.org/10.1038/s41598-020-70069-z

Russo A, Gouveia CM, Páscoa P, et al (2017) Assessing the role of drought events on wildfires in the Iberian Peninsula. Agric For Meteorol 237–238:50–59. https://doi.org/10.1016/j.agrformet.2017.01.021

Salis M, Ager AA, Arca B, et al (2013) Assessing exposure of human and ecological values to wildfire in Sardinia, Italy. Int J Wildland Fire 22:549–565. https://doi.org/10.1071/WF11060

Sánchez-Benítez A, García-Herrera R, Barriopedro D, et al (2018) June 2017: The Earliest European Summer Mega-heatwave of Reanalysis Period. Geophys Res Lett 45:1955–1962. https://doi.org/10.1002/2018GL077253

Sanderson BM, Wehner M, Knutti R (2017) Skill and independence weighting for multi-model assessments. Geosci Model Dev 10:2379–2395. https://doi.org/10.5194/gmd-10-2379-2017

San-Miguel-Ayanz J, Schulte E, Schmuck G, et al (2012) Comprehensive Monitoring of Wildfires in Europe: The European Forest Fire Information System (EFFIS). In: Approaches to Managing Disaster - Assessing Hazards, Emergencies and Disaster Impacts. IntechOpen

Soares PMM, Cardoso RM (2018) A simple method to assess the added value using high-resolution climate distributions: Application to the EURO-CORDEX daily precipitation. International Journal of Climatology 38:1484–1498. https://doi.org/10.1002/joc.5261

Soares PMM, Cardoso RM, Lima DCA, Miranda PMA (2017a) Future precipitation in Portugal: high-resolution projections using WRF model and EURO-CORDEX multi-model ensembles. Clim Dyn 49:2503–2530. https://doi.org/10.1007/s00382-016-3455-2

Soares PMM, Cardoso RM, Miranda PMA, et al (2012) WRF high resolution dynamical downscaling of ERA-Interim for Portugal. Clim Dyn 39:2497–2522. https://doi.org/10.1007/s00382-012-1315-2

Soares PMM, Lima DCA, Cardoso RM, et al (2017b) Western Iberian offshore wind resources: More or less in a global warming climate? Appl Energy 203:72–90. https://doi.org/10.1016/j.apenergy.2017.06.004

Soares PMM, Lima DCA, Cardoso RM, Semedo A (2017c) High resolution projections for the western Iberian coastal low level jet in a changing climate. Clim Dyn 49:1547–1566. https://doi.org/10.1007/s00382-016-3397-8

Sousa PM, Trigo RM, Pereira MG, et al (2015) Different approaches to model future burnt area in the Iberian Peninsula. Agric For Meteorol 202:11–25. https://doi.org/10.1016/j.agrformet.2014.11.018

Stocks BJ, Lynham TJ, Lawson BD, et al (1989) The Canadian Forest Fire Danger Rating System: An Overview. The Forestry Chronicle 65:450–457. https://doi.org/10.5558/tfc65450-6

Trigo IF, Bigg GR, Davies TD (2002) Climatology of cyclogenesis mechanisms in the Mediterranean. Mon Weather Rev 130:549–569. https://doi.org/10.1175/1520-0493(2002)130<0549:COCMIT>2.0.CO;2

Trigo IF, Dacamara CC, Viterbo P, et al (2011) The Satellite Application Facility for Land Surface Analysis. Int J Remote Sens 32:2725–2744. https://doi.org/10.1080/01431161003743199

Trigo RM, Pereira JMC, Pereira MG, et al (2006) Atmospheric conditions associated with the exceptional fire season of 2003 in Portugal. International Journal of Climatology 26:1741–1757. https://doi.org/10.1002/joc.1333

Trigo RM, Sousa PM, Pereira MG, et al (2016) Modelling wildfire activity in Iberia with different atmospheric circulation weather types. International Journal of Climatology 36:2761–2778. https://doi.org/10.1002/joc.3749

Trnka M, Možný M, Jurečka F, et al (2021) Observed and estimated consequences of climate change for the fire weather regime in the moist-temperate climate of the Czech Republic. Agric For Meteorol 310:108583. https://doi.org/10.1016/j.agrformet.2021.108583

Turco M, Jerez S, Augusto S, et al (2019) Climate drivers of the 2017 devastating fires in Portugal. Sci Rep 9:1–8. https://doi.org/10.1038/s41598-019-50281-2 van Vuuren DP, Edmonds J, Kainuma M, et al (2011) The representative concentration pathways: An overview. Clim Change 109:5–31. https://doi.org/10.1007/s10584-011-0148-z

van Wagner CE (1974) A spread index for crown fires in spring

van Wagner CE (1987) Development and structure of the Canadian Forest Fire Weather Index System

Varela V, Vlachogiannis D, Sfetsos A, et al (2019) Projection of forest fire danger due to climate change in the French Mediterranean region. Sustainability (Switzerland) 11:4284. https://doi.org/10.3390/su11164284

Vautard R, Gobiet A, Jacob D, et al (2013) The simulation of European heat waves from an ensemble of regional climate models within the EURO-CORDEX project. Clim Dyn 41:2555–2575. https://doi.org/10.1007/s00382-013-1714-z

Wenzel S, Eyring V, Gerber EP, Karpechko AY (2016) Constraining future summer austral jet stream positions in the CMIP5 ensemble by process-oriented multiple diagnostic regression. J Clim 29:673–687. https://doi.org/10.1175/JCLI-D-15-0412.1

Zhang X, Hegerl G, Zwiers FW, Kenyon J (2005) Avoiding inhomogeneity in percentile-based indices of temperature extremes. J Clim 18:1641–1651. https://doi.org/10.1175/JCLI3366.1

Supplementary Materials

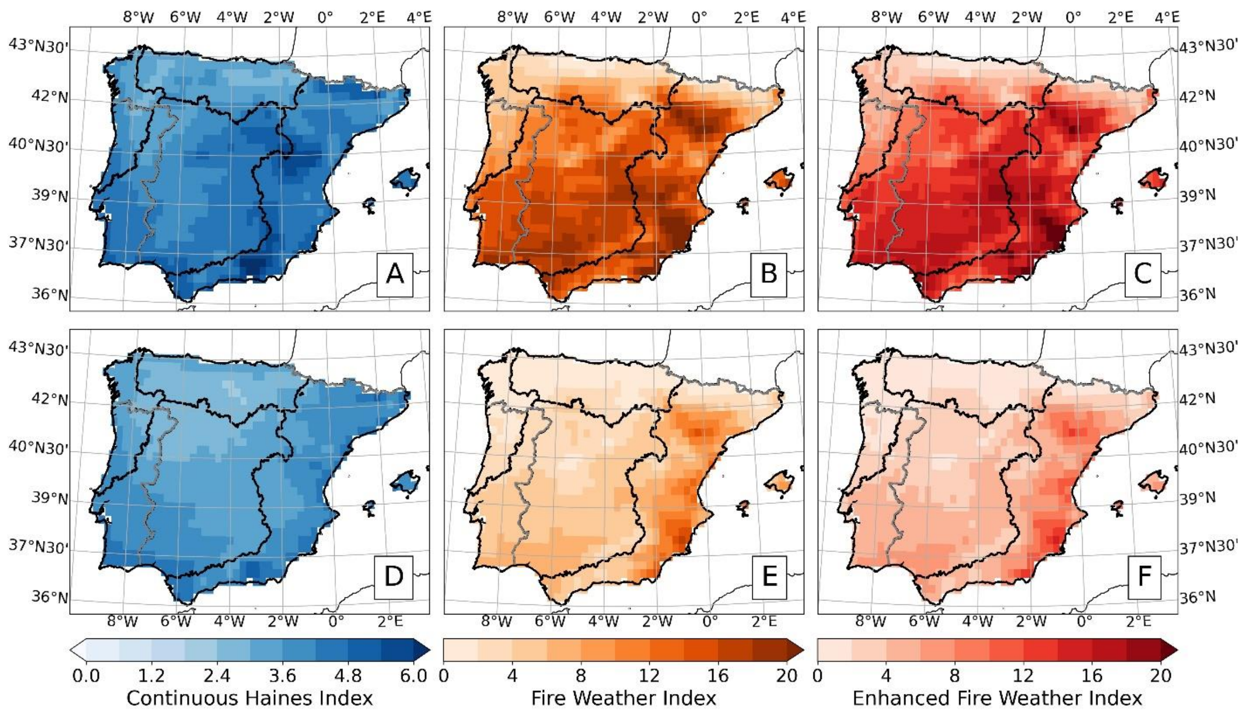

Figure S1 – Field climatology for the Iberian Peninsula for the 1980–2020 period for the three indexes (A) CHI, (B) FWI, and (C) FWIe.

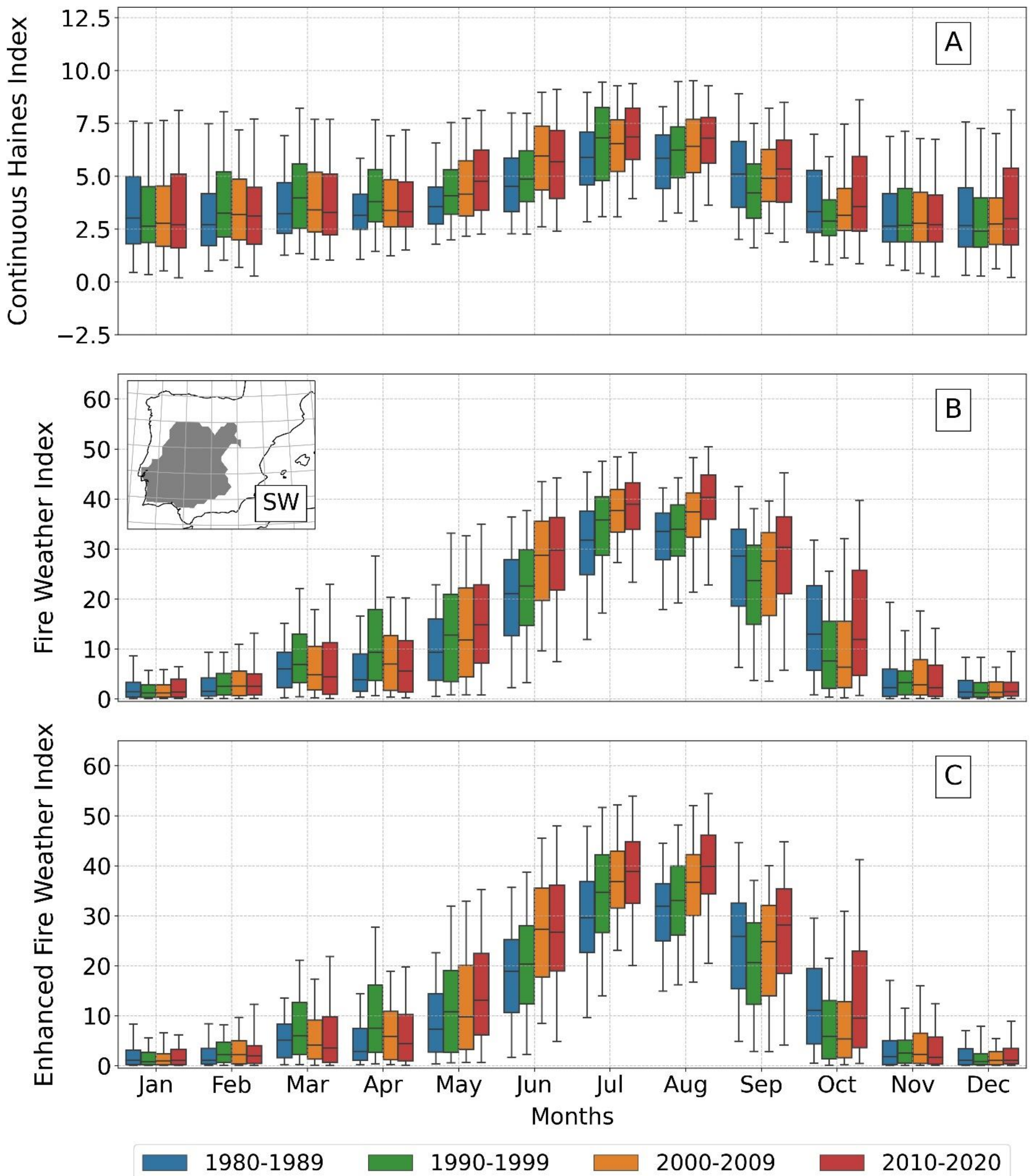

Figure S2 – Annual cycles for the SW cluster during the period 1980–2020 for CHI (top), FWI (middle), and FWIe (bottom).

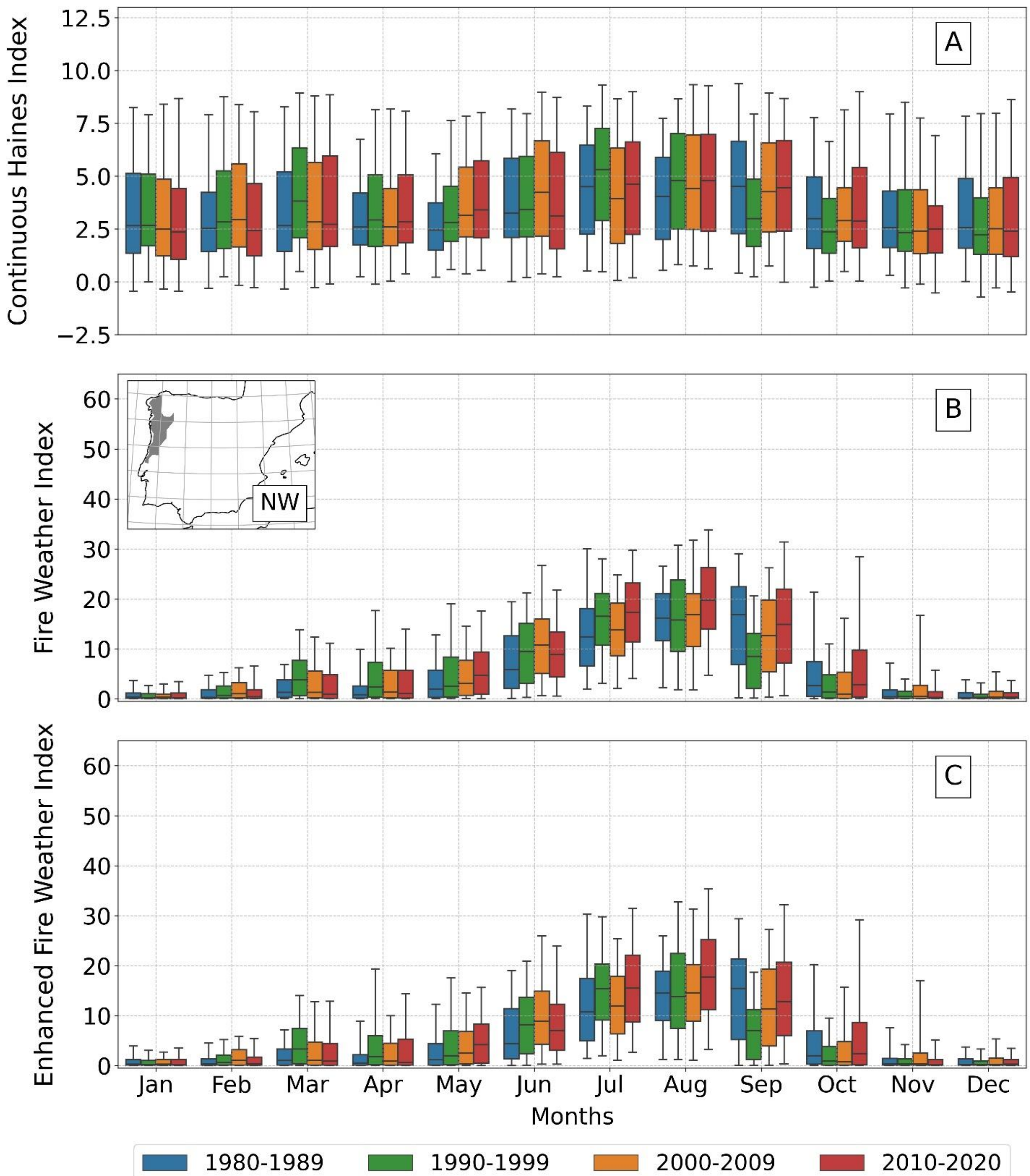

Figure S3 – As Figure S2 but for the NW cluster.

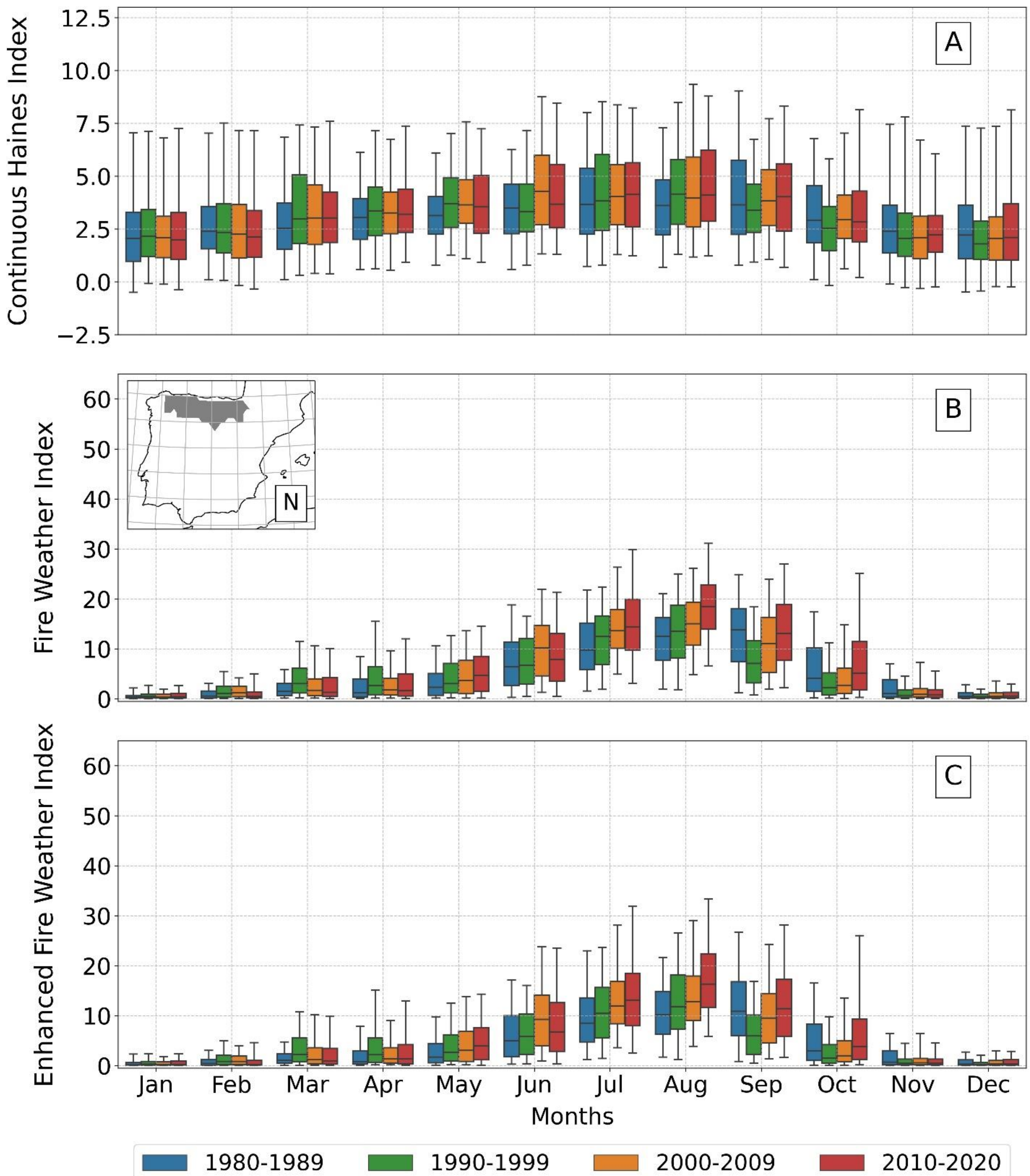

Figure S4 – As Figure S2 but for the N cluster.

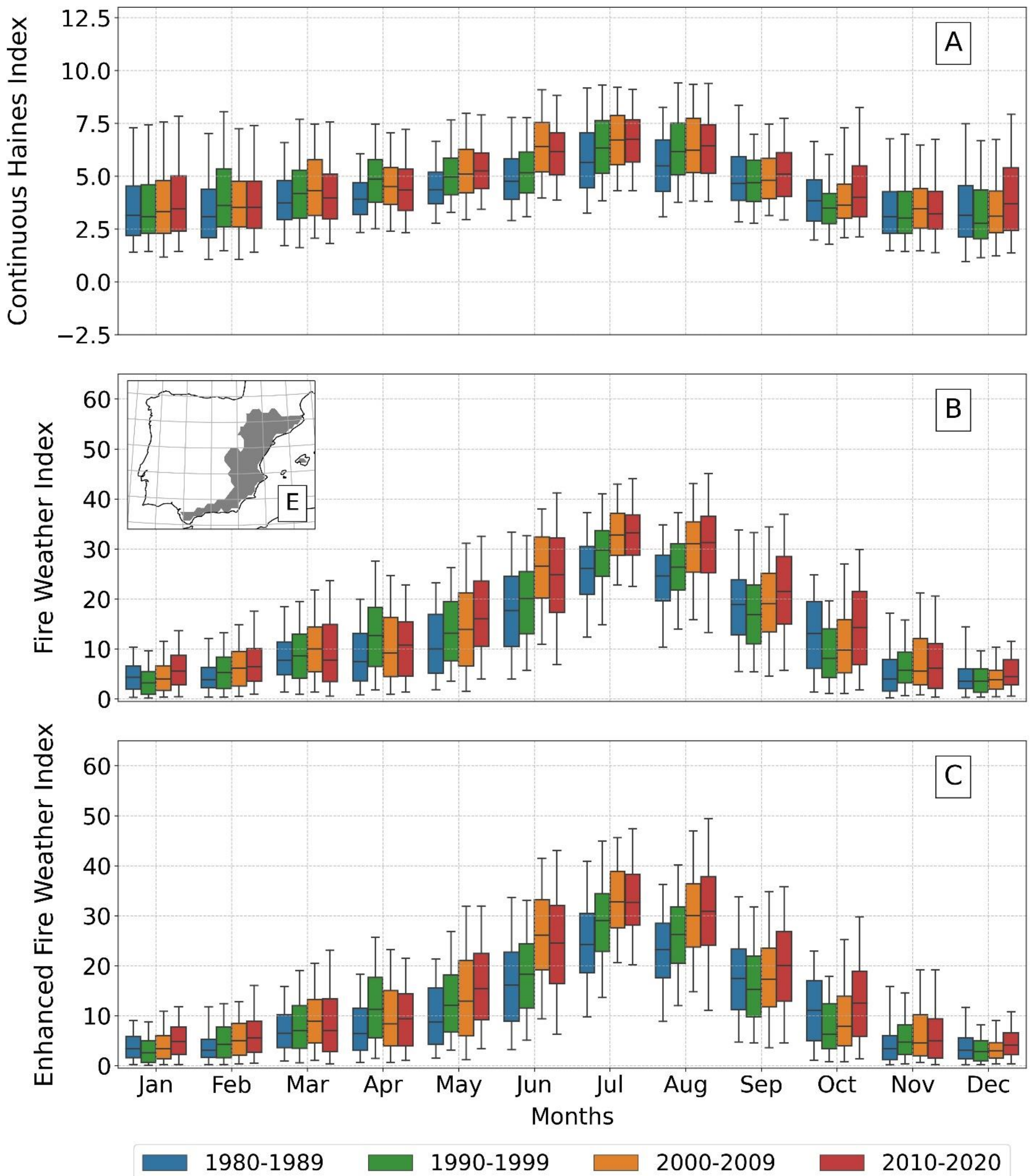

Figure S5 – As Figure S2 but for the E cluster.

Table S1 – Summary of statistics for CHI, FWI, and FWIe taking into account the complete year, summer, and winter. The statistics are divided into clusters SW, NW, N, and E.

	CHI			FWI			FWIe		
	All year	Summer	Winter	All year	Summer	Winter	All year	Summer	Winter
	Region SW								
Avg. Trend	0,141	0,255	0,021	0,194	1,954	0,003	0,131	2,216	0,000
% of significant pixels	100,000	99,800	25,300	92,000	100,000	7,330	70,700	100,000	0,900
	Region NW								
Avg. Trend	0,048	0,062	-0,011	0,000	0,570	0,000	0,000	0,439	0,000
% of significant pixels	77,200	49,400	12,700	1,270	98,700	0,000	0,000	96,700	0,000
	Region N								
Avg. Trend	0,076	0,150	0,022	0,040	0,890	0,000	0,012	0,814	0,000
% of significant pixels	76,600	66,200	40,900	39,600	90,300	0,600	13,000	77,920	0,700
	Region E								
Avg. Trend	0,175	0,259	0,100	0,587	1,922	0,253	0,524	2,130	0,206
% of significant pixels	98,700	96,700	92,600	95,500	96,500	71,400	95,500	97,400	66,900

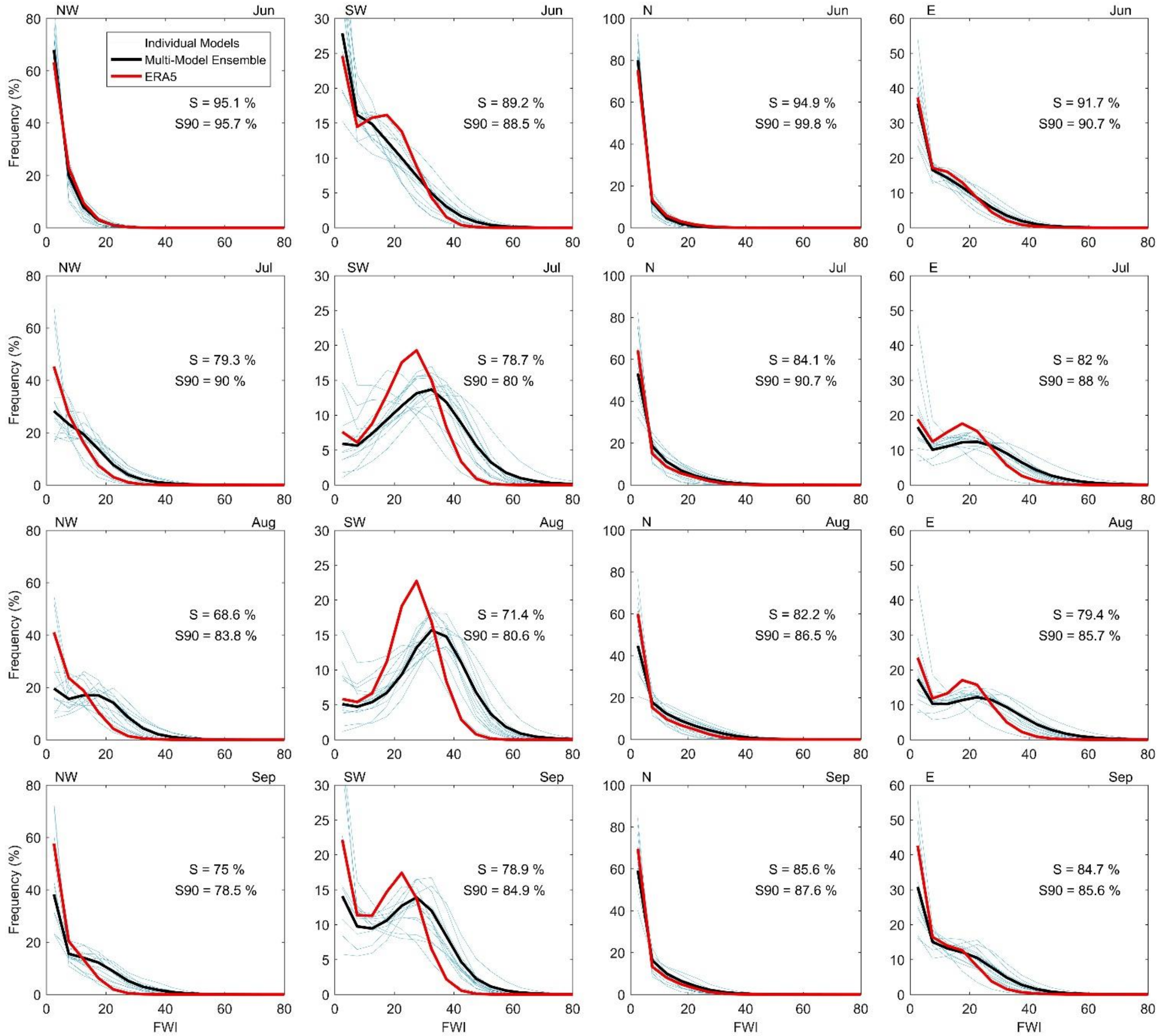

Figure S6 – FWI distributions from the multi-model ensemble (black lines) compared with those from ERA5 (red lines). The individual models' distributions are shown in light grey. The distributions are from June to September (top to bottom) and to clusters NW, SW, N, and E (left to right). Presented inside the plots are the respective S and S90 scores.

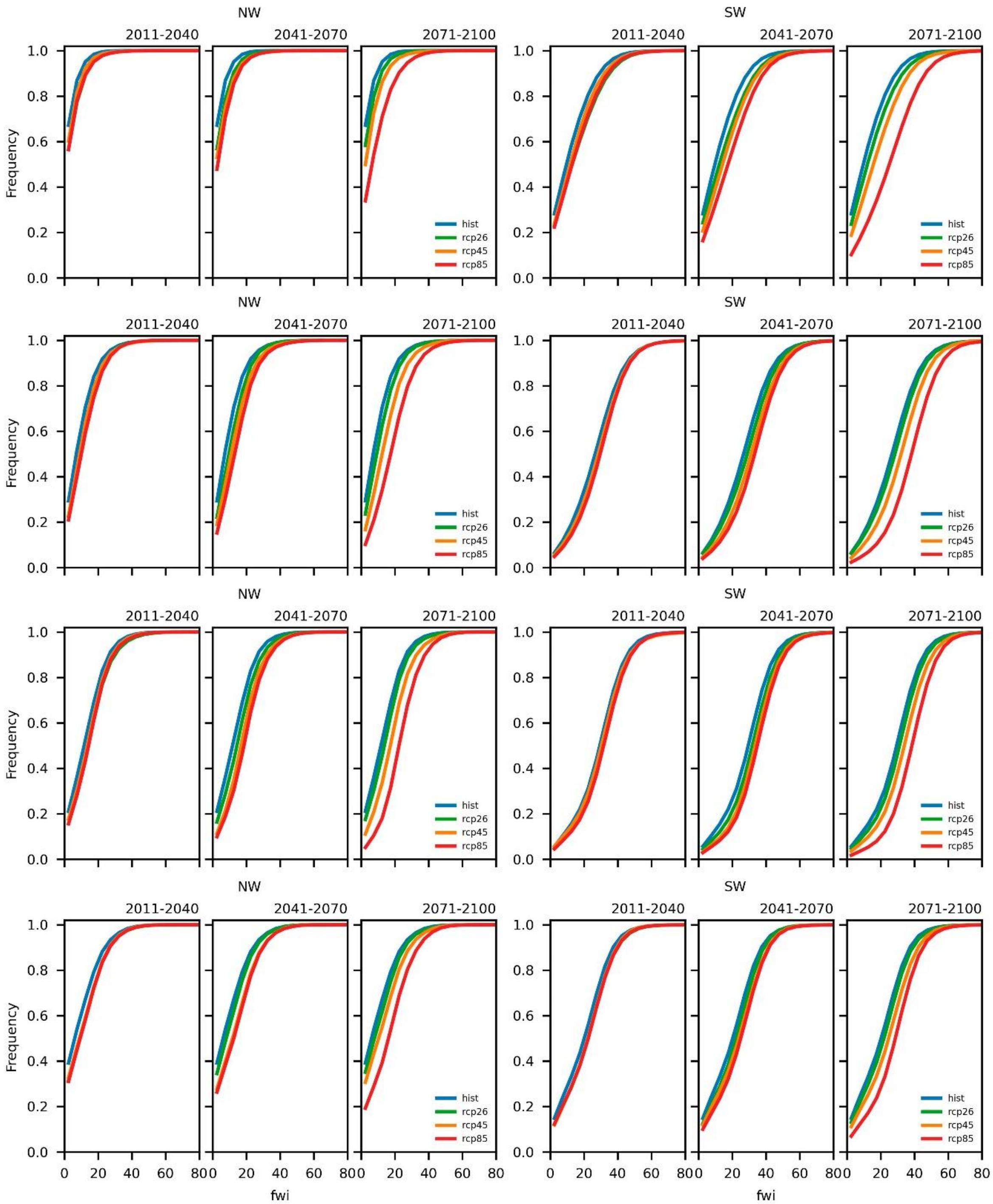

Figure S7a – CDFs of FWI for NW (left) and SW (right) for the months of JJAS (top to bottom).

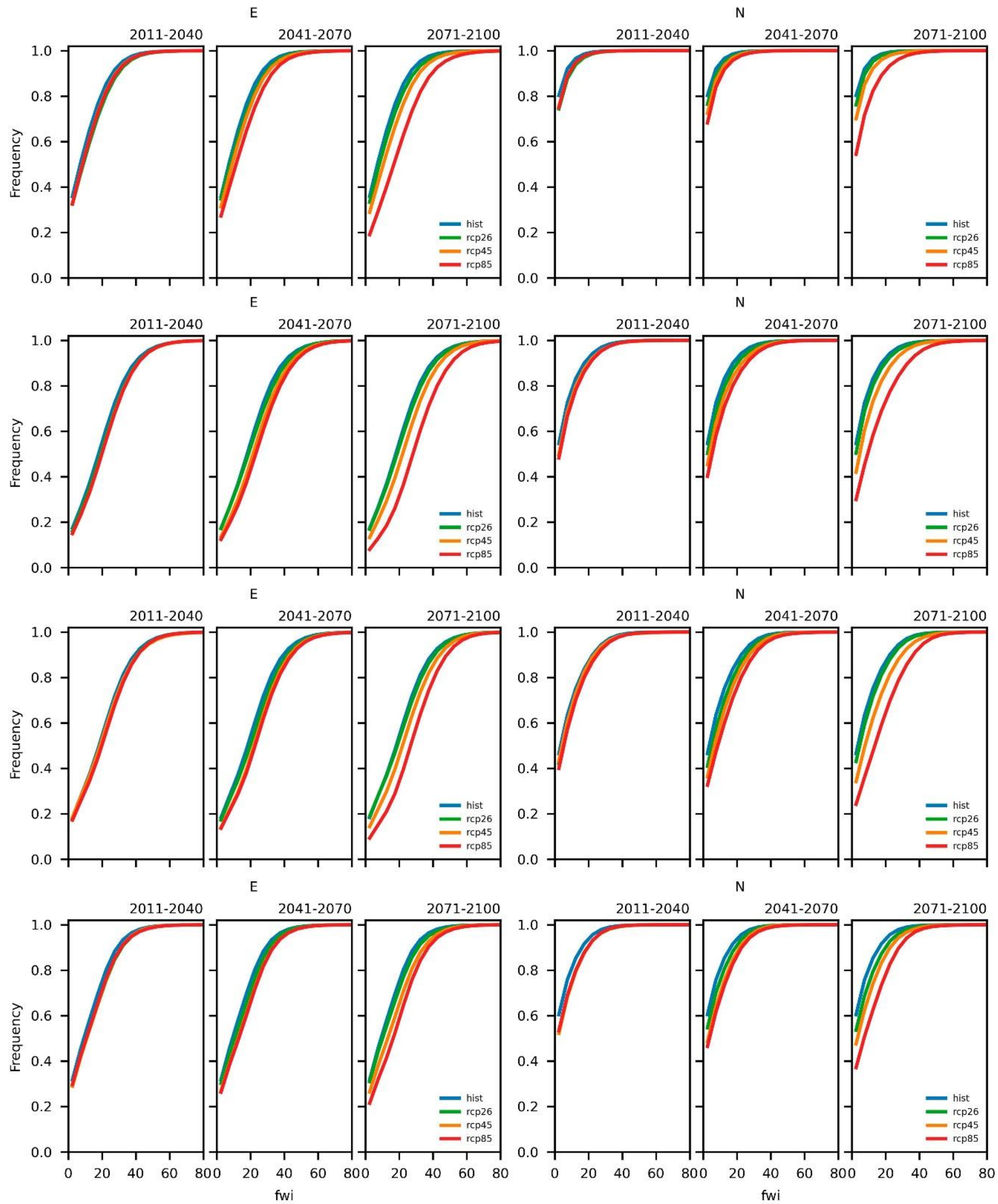

Figure S7b – CDFs of FWI for E (left) and N (right) for the months of JJAS (top to bottom).

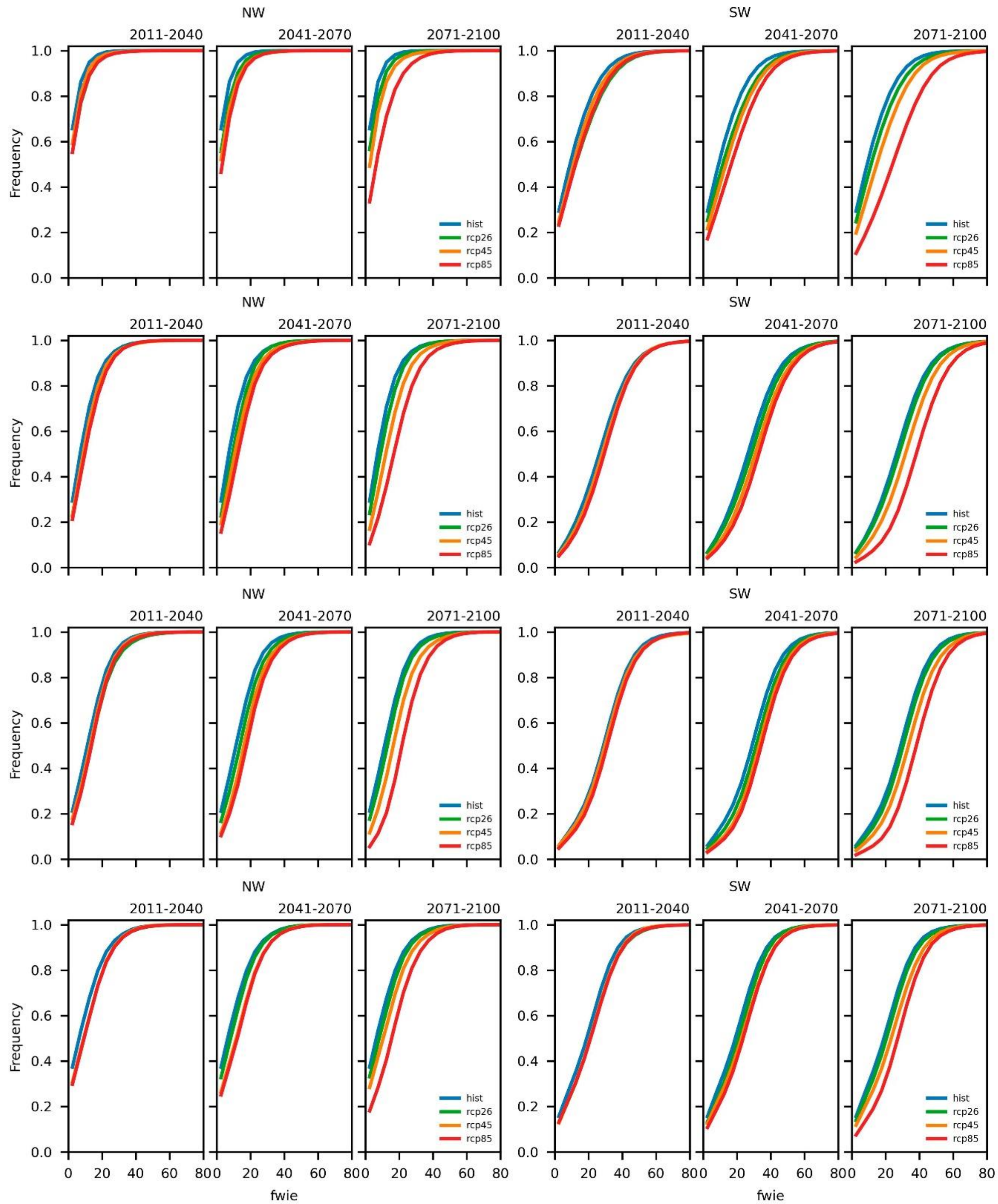

Figure S7c – CDFs of FWIe for NW (left) and SW (right) for the months of JJAS (top to bottom).

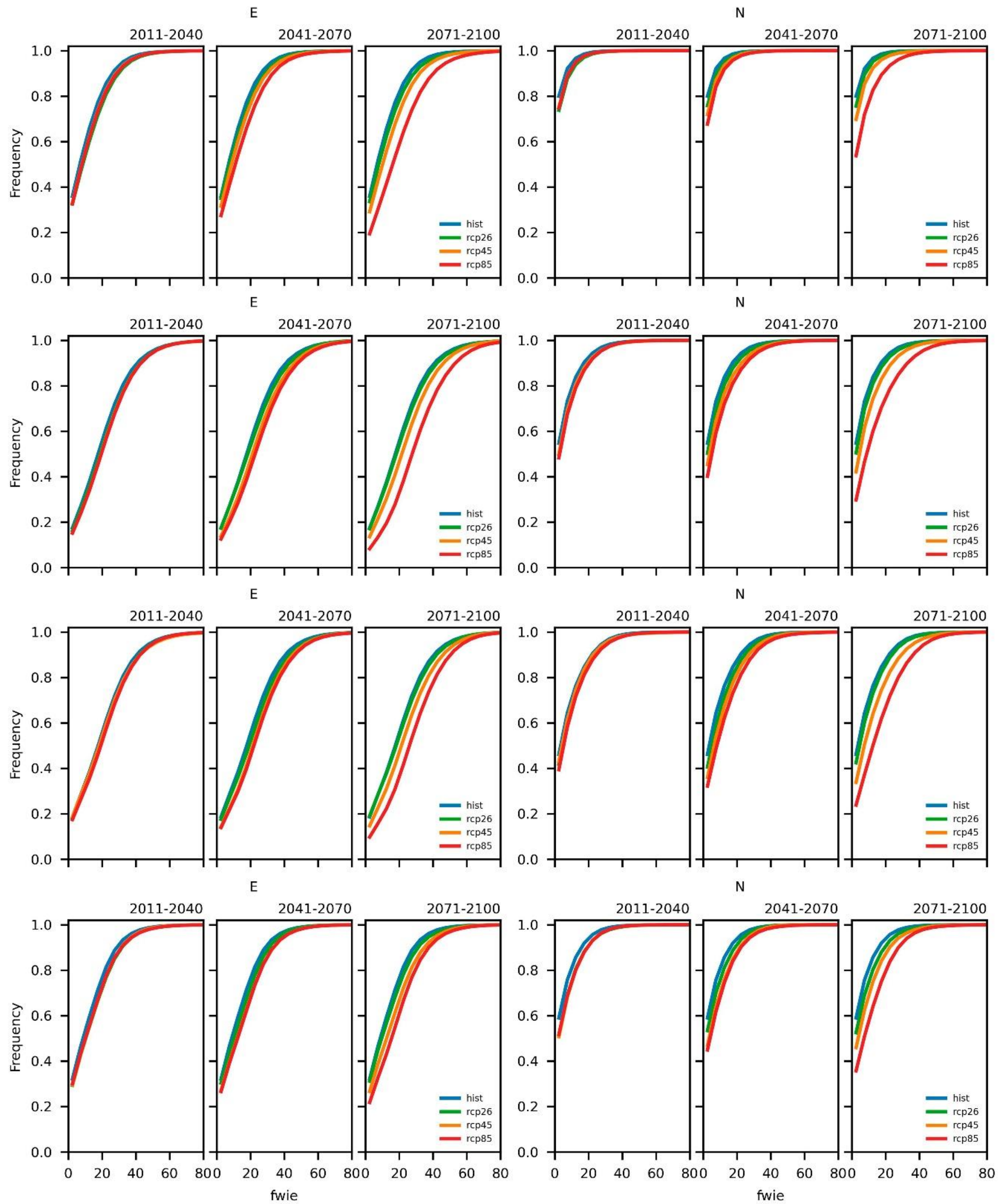

Figure S7d – CDFs of FWIe for E (left) and N (right) for the months of JJAS (top to bottom).